

1 **Conceptual models of dissolved carbon fluxes in a two-layer**
2 **stratified lake: interannual typhoon responses under extreme**
3 **climates**

4 Hao-Chi Lin¹, Keisuke Nakayama², Jeng-Wei Tsai³, and Chih-Yu Chiu⁴

5
6 ¹ Department of Bioenvironmental Systems Engineering, National Taiwan University,
7 Taipei City, Taiwan

8 ² Graduate School of Engineering, Kobe University, Kobe City, Japan

9 ³Graduate Institute of Bioresources, National Pingtung University of Science and
10 Technology, Pingtung, Taiwan

11 ⁴ Biodiversity Research Center, Academia Sinica, Taipei City, Taiwan

12 * Corresponding author: Keisuke Nakayama (nakayama@phoenix.kobe-u.ac.jp)

15 **Abstract**

16 Extreme climates affect the seasonal and interannual patterns of carbon (C) distribution
17 in lentic ecosystems due to the regimes of river inflow and thermal stratification. Typhoons
18 rapidly load substantial amounts of terrestrial C into smaller subtropical lakes (i.e., Yuan-Yang
19 Lake, YYL, Taiwan), renewing and mixing the water column. We developed a conceptual
20 dissolved C model and hypothesized that allochthonous C loading and river inflow intrusion may
21 affect the dissolved inorganic C (DIC) and dissolved organic C (DOC) distributions in a small
22 subtropical lake under these extreme climates. A two-layer conceptual C model was developed to
23 explore how the DIC and DOC fluxes respond to typhoon disturbances on seasonal and
24 interannual time scales in YYL while simultaneously considering autochthonous processes such
25 as algal photosynthesis, remineralization, and vertical transformation. To compare the temporal
26 patterns of fluxes between typhoon years (2015–2016) and non-typhoon years (2017–2018),
27 monthly field samples were obtained and their DIC, DOC, and chlorophyll *a* concentrations
28 measured. The results demonstrated that net ecosystem production was 3.14 times higher in the
29 typhoon years than in the non-typhoon years. This results suggested that a loading of
30 allochthonous C was the most crucial driver of the temporal variation of C fluxes in the typhoon
31 years because of changes in physical and biochemical processes, such as photosynthesis,
32 mineralization, and vertical transportation. However, the lowered vertical transportation rate
33 shaped the seasonal C in the non-typhoon years due to thermal stratification within this small
34 subtropical lake.

35

36 1. Introduction

37 The Intergovernmental Panel for Environmental Changes Sixth Assessment Report
38 (IPCC AR6 2021) suggested that, by 2050, not only is air temperature going to increase by at
39 least about 1.5°C but high-intensity storms and drought events will become more frequent as a
40 result of global warming and climate change. In freshwater ecosystems, extreme climates may
41 change the mixing regimes of freshwater columns (Kraemer et al., 2021; Maberly et al., 2020;
42 Woolway et al., 2020), heat wave events (Woolway et al., 2021a; Woolway et al., 2021b),
43 droughts (Marcé et al., 2019), and floods (Woolway et al., 2018). Freshwater ecosystems store
44 around 0.32 to 1.8 Pg C yr⁻¹, which is approximately equivalent to shallow coastal areas,
45 providing availability to food webs that support human resources, such as acting as processing
46 hotspots in regional carbon (C) cycling (Aufdenkampe et al., 2011; Cole et al., 2007; Engel et
47 al., 2018; Lauerwald et al., 2015; Raymond et al., 2013).

48 The responses of C fluxes in small lakes (lake area < 1 km²) are sensitive to climate
49 change due to the ease with which C mixes within water columns (Doubek et al., 2021;
50 MacIntyre et al., 2021; Winslow et al., 2015). Moreover, storms induce dramatic changes in
51 thermal stratification and water inflows (Lin et al., 2022; Olsson et al., 2022b; Vachon and Del
52 Giorgio, 2014; Woolway et al., 2018). River inflows and wind turbulence released
53 allochthonous C from sediments into the water column after storm events in small stratified
54 lakes (Bartosiewicz et al., 2015; Czikowsky et al., 2018; Vachon and Del Giorgio, 2014). Small
55 lakes account for 25% to 35% of the total area of the earth's surface lakes (Cole et al., 2007;
56 Downing et al., 2006; Raymond et al., 2013). Compared to the case in larger lakes, our
57 understanding of C fluxes in small lakes remain uncertain because small lakes have usually
58 been ignored in calculations of C fluxes on a global scale (Cole et al., 2007; Raymond et al.,
59 2013). Thus, elucidation of the C fluxes in small lakes in extreme weathers conditions is key to
60 optimizing estimations of global C fluxes in extreme climates.

61 Understanding the influences of physical, hydrological, and biogeochemical processes
62 on the fate of C fluxes in smaller lake ecosystems is challenging work (Aufdenkampe et al.,
63 2011; Cole et al., 2007; Raymond et al., 2013; Tranvik et al., 2009; Vachon et al., 2021;
64 Woolway et al., 2018). The physical and biogeochemical regimes under climate change remain
65 uncertain, such as biological compositions, mixing regimes, morphometric characteristics, and
66 air–water energy fluxes (evaporation and transpiration) (Woolway et al., 2020). Dissolved
67 inorganic carbon (DIC) concentration is an important factor in estimating CO₂ fluxes within
68 lake ecosystems (Smith, 1985). Among C fluxes in a freshwater body, the partial pressure of
69 CO₂ ($p\text{CO}_2$), defined as CO₂ emission across the air–water interface, is affected by DIC, water
70 temperature, wind speed, and pH (Jähne et al., 1987; Smith, 1985). River inflows, sediment C
71 burial, and heterotrophic respiration in the water column contribute to DIC dynamics in lakes

(Hope et al., 2004; Vachon et al., 2021); simultaneously, autotrophic organisms, such as plankton and submerged vegetation, capture DIC via photosynthesis (Amaral et al., 2022; Nakayama et al., 2020; Nakayama et al., 2022). Moreover, calcification and mineralization may consume dissolved oxygen within water, inducing uncertainty in $p\text{CO}_2$ estimation (Hanson et al., 2015; Lin et al., 2022; Nakayama et al., 2022). Dissolved organic carbon (DOC) might contribute to CO_2 emission from lake water to the atmosphere through mineralization and remineralization within lake ecosystems (Hanson et al., 2015; Sobek et al., 2005). In subtropical freshwater ecosystems, DOC concentration is a vital factor in describing variances in mineralization and remineralization rates for dissolved C (Lin et al., 2022; Shih et al., 2019).

Typhoons might significantly impact C distributions within the water columns in subtropical regions (Chiu et al., 2020; Lin et al., 2022). Kossin et al. (2013) investigated global storm events with an accumulated rainfall of about 50 mm, which accounts for approximately 10 %–40% of precipitation in a subtropical typhoon event. Some studies found not only that extreme rainstorms would impact the dissolved carbon in large lakes and catchments due to weathering (Sun et al., 2021; Zhou et al., 2023) but also that typhoon disturbances quickly mix, renew, or dilute the water in small subtropical lakes (Kimura et al., 2012; Kimura et al., 2017; Lin et al., 2022). However, the complex interactions between biogeochemical and physical regimes for autochthonous and allochthonous C introduce uncertainty in elucidating the complete patterns between typhoons and dissolved C concentrations in small subtropical lakes. This uncertainty hinders our understanding of the seasonal and interannual variations in DIC and DOC concentrations (Lin et al., 2022). Thus, to understand the seasonal regimes and to estimate C fluxes in subtropical lakes, we investigated the variations of DIC and DOC due to typhoon disturbances.

Typhoons' effects on C fluxes were previously studied in a small, two-layer stratified, subtropical lake, Yuan–Yang Lake (YYL) in Taiwan (Chiu et al., 2020; Jones et al., 2009; Lin et al., 2021; Lin et al., 2022). Jones et al. (2009) used the conceptual hydrology model and sensor data to estimate CO_2 emission in YYL during typhoon disturbances that occurred in October 2004: 2.2 to 2.7 $\text{g C m}^{-2} \text{ d}^{-1}$ of CO_2 was released into the atmosphere. CO_2 emissions into the atmosphere were recorded at around 3.0 to 3.7 $\text{g C m}^{-2} \text{ d}^{-1}$ in summer and autumn 2015 because of substantial loads of terrestrial C via river inflows after strong typhoons in YYL (Chiu et al., 2020). In particular, vertical mixing, thermal stratification, and river retention regimes were found to be essential physical processes in the C fluxes in YYL (Lin et al., 2021; Lin et al., 2022). The results of these studies suggest that river intrusion and thermal stratification are key factors shaping the seasonal and interannual patterns of C fluxes during typhoon disturbances. River intrusion controls not only the C fluxes, algal biomass, and nutrient loading, but also influences the length of stratification and hydraulic retention times (Lin et al., 2021; Lin et al.,

108 2022; Maranger et al., 2018; Nakayama et al., 2020; Olsson et al., 2022a; Olsson et al., 2022b;
109 Zwart et al., 2017; Vachon and Del Giorgio, 2014). Therefore, we hypothesized that
110 allochthonous C loading and river inflow intrusion might affect DIC and DOC distributions.
111 Further, autochthonous processes in small subtropical lakes, such as algal photosynthesis,
112 remineralization, and vertical transportation, must also be considered. Here, we tested our
113 hypothesis developing two-layer conceptual C models to assess C flux responses to typhoon
114 disturbances in small subtropical lakes.

116 **2. Materials and methods**

117 **2.1 Study site**

118 YYL is a shallow (mean water depth: 4.3 m) and oligotrophic (total phosphorous: 10-
119 20 $\mu\text{g-P L}^{-1}$; total nitrogen: 20-60 $\mu\text{g-N L}^{-1}$) subtropical mountain lake (Chou et al., 2000; Tsai
120 et al., 2008; Wu et al., 2001) on Chi-Lan Mountain at around 1,640 asl in north-central Taiwan
121 (24.58° N, 121.40° E) (Fig. 1). Its water is brown because of humic acid content (colored
122 dissolved organic matter: 20–50 ppb QSE; with specific ultraviolet absorbance at 254 nm
123 assessed by a portable fluorometer (model C3; Turner Designs, Sunnyvale, CA, USA); mean
124 pH: 5.4). YYL is surrounded by old-growth trees such as *Chamaecyparis formosensis*,
125 *Chamaecyparis obtusa* var. *formosana*, and *Rhododendron formosanum* Heiml (Chou et al.,
126 2000). Precipitation is over 3,000 mm yr^{-1} , and typhoon precipitation contributes up to half of
127 the total precipitation in YYL annually (Chang et al., 2007; Lai et al., 2006). Due to the rapid
128 renewal of the water body, the water retention time (or residence time) was around 4.4 days in
129 typhoon Megi from 27 September to 1 October 2016 (Lin et al., 2022). The water surface
130 temperature ranges from 15 to 25 °C during March to August, and the water column overturns
131 in September (Kimura et al., 2012; Kimura et al., 2017; Lin et al., 2021). The concentrations of
132 DIC, DOC (Lin et al., 2021), total nitrogen, total phosphate (Chiu et al., 2020; Tsai et al., 2008)
133 and bacteria compositions (Shade et al., 2011) increase within YYL from autumn to winter.
134 YYL has been registered as a long-term ecological study site by the Ministry of Science and
135 Technology (MOST) of Taiwan since 1992 and it became part of the Global Lake Ecological
136 Observatory Network (GLEON) in 2004.

138 **2.2 Water sampling and chemical analysis**

139 We collected water quality samples (DOC, DIC, and Chl. *a*) at water depths of 0.04,
140 0.50, 1.00, 2.00, and 3.50 m at the buoy site (Fig. 1). From January 2015 to December 2018, we
141 measured the water surfaces for six river inflows and one outflow each month using a horizontal
142 van Dorn bottle (2.20 L, acrylic) (Fig. 1). These liquid samples were collected using a portable

143 hand pump and glass microfiber filter papers (47 mm GF/F, nominal pore size 0.70 μm ;
144 Whatman, Maidstone, Kent, UK) to obtain filtrate samples. Water samples were stored at
145 around 4°C in a refrigerator until analysis. Samples were analyzed using an infrared gas detector
146 to detect DIC and DOC concentrations with persulfate digestion (model 1088 Rotary TOC
147 autosampler; OI Analytical, College Station, TX, USA). The filter papers were kept refrigerated
148 in opaque bottles at around -25 °C in a refrigerator until the samples were analyzed. In the
149 laboratory, the filter papers were extracted with methanol to obtain Chl. *a* concentration using a
150 portable fluorometer (model 10-AU-005-CE; Turner Designs, Sunnyvale, CA, USA), with
151 specific wavelengths were 430 nm (blue) and 662 nm (red). All analysis was completed within
152 72 hours of exposure to light to reduce the degradation.

153

154 **2.3 Data analysis and numerical modeling**

155 Three water quality variables (DIC, DOC, and Chl. *a*) were compared between different
156 layers (upper and lower layers), years (typhoon and non-typhoon years), and seasons (spring,
157 summer, autumn, and winter). First, we separated our investigation data into typhoon years and
158 non-typhoon years as described in Sect. 2.3.1. Next, to simulate the DIC and DOC concentration
159 under extreme weather scenarios in YYL, we developed a conceptual equations model to generate
160 continuous DIC and DOC data at the upper and lower layers, as shown in Sect. 2.3.2. This also
161 helped us understand the transportation, photosynthesis, and remineralization rates between
162 seasons and between typhoon and non-typhoon years.

163

164 **2.3.1 Typhoon and non-typhoon years**

165 We collected meteorological data from a tower located about 1.0 km from YYL (Lin et
166 al., 2021; Lin et al., 2022). Data on rainfall (model N-68; Nippon Electric Instrument, Tokyo,
167 Japan) and wind speed (model 03001, R.M. Young, Traverse City, MI, USA) were stored in a
168 datalogger (model CR1000; Campbell Scientific, Logan, UT, USA) every 10 min. River discharge
169 (Q_{in} , $\text{m}^3 \text{ d}^{-1}$) was estimated every 10 min using the rainfall data and a water depth meter (model
170 HOBO U20; Onset Computer, Bourne, MA, USA) at the end of a river inflow (Fig. 1) using the
171 Manning formula. Transparency was estimated using Secchi disc data measured at a certain
172 interval in that time frame from 10:00 to 14:00 (GMT+08:00).

173 As Table 1 shows, four strong typhoons were recorded by using wind speed and rainfall
174 meteorological parameters, contributing a total of 2,254 mm of precipitation in all 24 months of
175 2015 and 2016; this accounted for 35.6% of across two years of typical rainfall ($> 3000 \text{ mm yr}^{-1}$).
176 However, no typhoon rainfall was recorded at YYL in 2017 and 2018; the total precipitation
177 was around $1,398 \text{ mm yr}^{-1}$, below half of average years. The annual average wind speed from
178 2015 to 2016 was higher by 0.09 m s^{-1} than in 2017 and 2018 (Table 1). Despite no significant

179 difference in average water depth between 2017 and 2018, the average discharge in 2015 and
 180 2016 was higher than $774 \text{ m}^3 \text{ d}^{-1}$ in 2017 and 2018 (Table 1). Thus, we considered 2015 and 2016
 181 as typhoon years and 2017 and 2018 as non-typhoon years.

182

183 2.3.2 **Conceptual two-layer DIC and DOC model**

184 Nakayama et al. (2010) successfully developed a conceptual two-layer dissolved oxygen
 185 model based on strong wind turbulence at Tokyo Bay. Lin et al. (2021) pointed out that thermal
 186 stratification that inhibits vertical C flux between the upper and lower layers in shallow stratified
 187 lakes makes it possible to develop conceptual two-layer C models (Lin et al., 2022; Nakayama et
 188 al., 2022). The phytoplankton and remineralization effects on DIC and DOC fluxes ($d\text{DIC}/dt$ and
 189 $d\text{DOC}/dt$, $\text{mg-C L}^{-1} \text{ d}^{-1}$) were considered in a conceptual two-layer equation model as shown in
 190 Equations 1–4. The fluxes in the upper layer (from the water surface to 2.5 m water depth) were
 191 calculated as follows:

$$V_U \frac{d\text{DIC}_U}{dt} = Q_U \text{DIC}_R - Q_{out} \text{DIC}_U - V_U \alpha_{PU} \text{Chl}_U + V_U \alpha_{MU} \text{DOC}_U + A_I w_I (\text{DIC}_L - \text{DIC}_U) + Q_L \text{DIC}_L - \frac{A_s F_{CO2}}{C_U} + P a_U \quad (1)$$

$$V_U \frac{d\text{DOC}_U}{dt} = Q_U \text{DOC}_R - Q_{out} \text{DOC}_U - V_U \alpha_{MU} \text{DOC}_U + A_I w_I (\text{DOC}_L - \text{DOC}_U) + Q_L \text{DOC}_L + P b_U \quad (2)$$

192 Those in the lower layer (from 2.5 to 4.0 m water depth) were calculated as follows:

$$V_L \frac{d\text{DIC}_L}{dt} = Q_L \text{DIC}_R - V_L \alpha_{PL} \text{Chl}_L + V_L \alpha_{ML} \text{DOC}_L + A_I w_I (\text{DIC}_U - \text{DIC}_L) - Q_L \text{DIC}_L + \frac{A_B B F_{DIC}}{C_U} + P a_L \quad (3)$$

$$V_L \frac{d\text{DOC}_L}{dt} = Q_L \text{DOC}_R - V_L \alpha_{ML} \text{DOC}_L + A_I w_I (\text{DOC}_U - \text{DOC}_L) - Q_L \text{DOC}_L + P b_L \quad (4)$$

$$V_{total} = V_U + V_L \quad (5)$$

$$Q_{in} = Q_U + Q_L \quad (6)$$

193 where, as shown in Table 2, total lake volume (V_{total} , $53,544 \text{ m}^3$) comprises to the upper layer
 194 (V_U , $45,456 \text{ m}^3$) and to the lower layer (V_L , $8,808 \text{ m}^3$) (Equation 5), and where the lake surface
 195 area (A_s) is $36,000 \text{ m}^2$ and the bottom of the lake area (A_B) is $3,520 \text{ m}^2$. The interface is 2.5 m
 196 vertically, and the interface area (A_I) is $7,264 \text{ m}^2$ in YYL. The water depth varied from 4.56 to

197 4.66 m during the typhoon period (Chiu et al., 2020; Lin et al., 2022). Therefore, we can assume
198 that the changes in lake volumes and areas were negligible. The coefficient C_U , with a value of
199 1000, was used to establish a standard unit for F_{CO_2} ($\text{mg-C m}^{-2} \text{ d}^{-1}$), considering the air–water
200 CO_2 exchange by Fick’s law as follows:

$$F_{CO_2} = k_{CO_2} \cdot K_H (pCO_2_{water} - pCO_2_{air}) \quad (7)$$

201 where k_{CO_2} is the gas transfer velocity from empirical wind speed equations (Cole and Caraco,
202 1998; Jähne et al., 1987; Smith, 1985; Wanninkhof, 1992). K_H is Henry’s coefficient calculated
203 by water temperature empirical equations (Plummer and Busenberg, 1982). pCO_2_{air} (μatm) is
204 the CO_2 partial pressure in the atmosphere using air pressure data (Lin et al., 2021; Lin et al.,
205 2022), and the atmospheric CO_2 concentration is assumed to be 400 ppm. pCO_2_{water} (μatm) is
206 the CO_2 partial pressure at the water surface around 0.04 m water depth from water quality data
207 (temperature, pH, and DIC concentrations). The empirical equation (Cai and Wang, 1998) was
208 also followed by Lin et al. (2021). F_{CO_2} contributed approximately half of the net ecosystem
209 production (NEP) across the water surface to the atmosphere in YYL (Lin et al., 2021). Further,
210 because sediment carbon may be an important flux into shallow subtropical lakes, the sediment
211 C flux (BF_{DIC} , BF_{DOC} , mg-C L^{-1}) in the lower layer was considered (Lin et al., 2022).

212 We assumed that the river discharge and outflow discharge (Q_{out} , $\text{m}^3 \text{ d}^{-1}$) are in a
213 quasi–steady state ($Q_{in} = Q_{out}$), divided into upper discharge (Q_U , $\text{m}^3 \text{ d}^{-1}$) and lower discharge
214 (Q_L , $\text{m}^3 \text{ d}^{-1}$) (Equation 6). Lin et al. (2021) showed that the buoyancy frequencies in YYL were
215 $0.011 \pm 0.004 \text{ s}^{-1}$, $0.013 \pm 0.004 \text{ s}^{-1}$, $0.006 \pm 0.003 \text{ s}^{-1}$, and $0.007 \pm 0.004 \text{ s}^{-1}$ from spring
216 (March–May), summer (June–August), autumn (September–November), and winter
217 (December–February), respectively, inhibiting the vertical profile of DIC mixed due to
218 stratification. We estimated the percentages of Q_U and Q_L based on the buoyancy frequency
219 following Lin et al. (2020 and 2022). Q_U values were 75%, 80%, 45%, and 50% of Q_{in} for
220 spring to winter, and Q_L values were 25%, 20%, 55%, and 50% of Q_{in} (Table 2).

221 Extreme weather events might induce stronger seasonal thermal stratification from
222 spring to summer and longer overturns from autumn to winter, thereby changing C distribution
223 and transportation within water bodies (Kraemer et al., 2021; Olsson et al., 2022a; Woolway et
224 al., 2020). Thus, we attempted to simulate extreme climate scenarios; we shifted the ratio of
225 Q_{in} for each season and tested the river intrusion hypothesis. We established two extreme
226 conditions: *Level 1* and *Level 2*. *Level 2* is the more extreme condition: Q_U is 80% (spring),
227 85% (summer), 50% (autumn), and 50% (winter) of Q_{in} ; Q_L is 20% (spring), 15% (summer),
228 50% (autumn), and 50% (winter) of Q_{in} . *Level 1* is the condition between the present and the
229 *Level 2* condition: Q_U is 77% (spring), 82% (summer), 47% (autumn), and 50% (winter) of
230 Q_{in} ; Q_L is 23% (spring), 18% (summer), 53% (autumn), and 50% (winter) of Q_{in} (Table 2).

231 The contributions of photosynthesis production depended on the chlorophyll *a*

concentration (Chl_U , Chl_L , mg L⁻¹) and on the absorption coefficients in the upper layer (α_{PU} , d⁻¹) and lower layer (α_{PL} , d⁻¹). The coefficients of DOC remineralization rates in the upper layer (α_{MU} , d⁻¹) and lower layer (α_{ML} , d⁻¹) were also considered in the conceptual models. The Pa_U , Pa_L , Pb_U , and Pb_L are constants in the conceptual models. To obtain unknown values (α_{PU} , α_{MU} , α_{PL} , α_{ML} , w_I , BF_{DIC} , BF_{DOC} , Pa_U , Pa_L , Pb_U , and Pb_L), we applied multiple linear regression analysis. Further, these unknown values were tested by trial and error to obtain the parameters of the *best-fit* condition (Nakayama et al., 2022). The same parameters of the *best-fit* condition were used to obtain the extreme conditions for *Level 1* and *Level 2*. We used the coefficient of determination (R^2) and the Nash–Sutcliffe model efficiency coefficient (NSE) (Nash and Sutcliffe, 1970) to quantify the performance of the equation model with DIC and DOC sampling data (observation data) for each simulation as follows.

$$NSE = 1 - \frac{\sum_{i=1}^n (Obs_i - Sim_i)^2}{\sum_{i=1}^n (Obs_i - \bar{Obs})^2} \quad (8)$$

where Obs is observation data of DIC and DOC concentrations, and Sim is best-fit data for conceptual model.

2.3.3 DIC and DOC fluxes

Net ecosystem production was defined as the difference between primary production and ecological respiration (NEP = GPP - ER) due to photosynthesis and respiration via biota (Dodds and Whiles, 2020). Given that we assumed that the C fluxes were dependent on the river inflows in YYL (Fig. 1), we estimated the NEP by end-member analysis using the C concentration of the river inflow and outflow (Lin et al., 2021; Nakayama et al., 2020) by following Equations 9–12. The upper layer NEP of DIC flux (mg C d⁻¹) was obtained from Equation 1 as follows:

$$\begin{aligned} \text{Upper flux}_{DIC} &= C_U \alpha_{PU} Chl_U - C_U \alpha_{MU} DOC_U - C_U \frac{A_I w_I (DIC_L - DIC_U)}{V_U} - C_U \frac{Pa_U}{V_U} \\ &= C_U \frac{Q_U DIC_R + Q_L DIC_L - Q_{out} DIC_U}{V_U} - \frac{A_S}{V_U} F_{CO2} \\ &= C_U \frac{1}{t_{rU}} \left(\frac{Q_U}{Q_{in}} DIC_R + \frac{Q_L}{Q_{in}} DIC_L - DIC_U \right) - F_C \\ t_{rU} &= \frac{V_U}{Q_{in}} \end{aligned} \quad (9)$$

The upper layer flux of DOC flux (mg C m⁻³ d⁻¹) was estimated from Equation 2:

$$\begin{aligned}
\text{Upper flux}_{\text{DOC}} &= C_U \alpha_{MU} \text{DOC}_U - C_U \frac{A_I w_I (\text{DOC}_L - \text{DOC}_U)}{V_U} - C_U \frac{Pb_U}{V_U} \\
&= C_U \frac{Q_U \text{DOC}_R + Q_L \text{DOC}_L - Q_{out} \text{DOC}_U}{V_U} \\
&= C_U \frac{1}{t_{rU}} \left(\frac{Q_U}{Q_{in}} \text{DOC}_R + \frac{Q_L}{Q_{in}} \text{DOC}_L - \text{DOC}_U \right)
\end{aligned} \tag{10}$$

255

256 The lower layer flux of DIC flux ($\text{mg C m}^{-3} \text{ d}^{-1}$) was estimated from Equation 3:

$$\begin{aligned}
\text{Lower flux}_{\text{DIC}} &= C_U \alpha_{PL} \text{Chl}_L - C_U \alpha_{ML} \text{DOC}_L - C_U \frac{A_I w_I (\text{DIC}_U - \text{DIC}_L)}{V_L} - \frac{A_B B F_{\text{DIC}}}{V_L} \\
&\quad - C_U \frac{P a_L}{V_L} = C_U \frac{Q_L (\text{DIC}_R - \text{DIC}_L)}{V_L} = C_U \frac{1}{t_{rL}} \frac{Q_L}{Q_{in}} (\text{DIC}_R - \text{DIC}_L) \\
t_{rL} &= \frac{V_L}{Q_{in}}
\end{aligned} \tag{11}$$

257

258 The lower layer flux of DOC flux ($\text{mg C m}^{-3} \text{ d}^{-1}$) was estimated from Equation 4:

$$\begin{aligned}
\text{Lower flux}_{\text{DOC}} &= C_U \alpha_{ML} \text{DOC}_L - C_U \frac{A_I w_I (\text{DOC}_U - \text{DOC}_L)}{V_L} - \frac{A_B B F_{\text{DOC}}}{V_L} - C_U \frac{Pb_L}{V_L} \\
&= C_U \frac{Q_L (\text{DOC}_R - \text{DOC}_L)}{V_L} = C_U \frac{1}{t_{rL}} \frac{Q_L}{Q_{in}} (\text{DOC}_R - \text{DOC}_L)
\end{aligned} \tag{12}$$

259

260 Thus, the total flux of DIC and that of DOC are:

$$\text{Flux}_{\text{DIC}} = \frac{V_U \text{Upper flux}_{\text{DIC}} + V_L \text{Lower flux}_{\text{DIC}}}{V_{total}} \tag{13}$$

$$\text{Flux}_{\text{DOC}} = \frac{V_U \text{Upper flux}_{\text{DOC}} + V_L \text{Lower flux}_{\text{DOC}}}{V_{total}} \tag{14}$$

261

262 where, F_C is $\frac{A_S}{V_U} F_{CO_2}$ and t_{rU} , t_{rL} are residence times (d) in the upper and lower layers,

263 respectively. These parameters were used for the best-fit condition as shown in Table 2.

264

265 **3. Results**

266 **3.1 Measurment data (monthly DIC, DOC, and Chl. a concentrations) in**
267 **typhoon and non-typhoon years**

268 The comparisons between the two typhoon years (2015 and 2016) revealed no
269 significant differences in DIC, DOC, and Chl *a* concentrations between the upper and lower layers;
270 however, all these parameters differed significantly between the layers in the non-typhoon years
271 2017 and 2018 (Fig. 2). This is because of typhoon-induced mixing and lower thermal
272 stratification between upper and lower layer(Lin et al., 2021; Lin et al., 2022). Overall, the average
273 DIC_U was 2.06 mg-C L⁻¹, and DIC_L was 3.66 mg-C L⁻¹; the average DOC_U was 5.87 mg-C L⁻¹,
274 and DOC_L was 8.02 mg-C L⁻¹; and Chl_U and Chl_L were 2.13 μ g-C L⁻¹ and 18.5 μ g-C L⁻¹,
275 respectively. In typhoon years, the average DIC_U was 2.34 mg-C L⁻¹, and DIC_L was 4.07 mg-C
276 L⁻¹; the average DOC_U was 6.10 mg-C L⁻¹, and DOC_L was 8.38 mg-C L⁻¹; and the Chl_U and
277 Chl_L were 2.38 μ g-C L⁻¹ 12.2 μ g-C L⁻¹, respectively (Fig. 2); In non-typhoon years, the average
278 DIC_U was 1.81 mg-C L⁻¹, and DIC_L was 3.28 mg-C L⁻¹; the average DOC_U was 5.66 mg-C L⁻¹,
279 and DOC_L was 7.67 mg-C L⁻¹; and Chl_U and Chl_L were 1.89 μ g-C L⁻¹ and 24.4 μ g-C L⁻¹,
280 respectively (Fig. 2).

281 ANOVA results indicated no significant differences in DIC concentrations among
282 seasons during the typhoon years (*p*-values ≥ 0.05), suggesting a lack of statistically significant
283 variation in DIC data across seasons (Fig. 3a–b). However, the DOC concentration showed
284 significant differences between seasons in the typhoon years (Fig. 3c–d). No significant
285 differences between Chl_U and Chl_L were observed among the seasons (Fig. 3e–f), whereas the
286 standard deviations (SD) of DIC and DOC were higher in summer and autumn (Fig. 3) due to
287 terrestrial C loading (Chiu et al., 2020). In summer, the SD values of DIC_U and DOC_U were
288 3.51 mg-C L⁻¹ and 3.69 mg-C L⁻¹, respectively (Fig. 3a, c, e). In autumn, DIC_L and DOC_L had
289 the highest SD (4.06 and 4.17 mg-C L⁻¹, respectively) (Fig. 3b, d). Notably, the maximums of
290 DIC_U and DOC_U were 7.06 and 15.6 mg-C L⁻¹ and those of DIC_L and DOC_L were 10.9 and
291 19.8 mg-C L⁻¹, respectively, in the typhoon years (Fig. 3a-d).

292 Positive Pearson correlations of 0.45 to 0.80 were observed between the DOC and DIC
293 in the typhoon years (Fig. 4a). In the non-typhoon years, the upper layer DIC_L was the only
294 variable correlated negatively with DOC in the upper and lower layers (Fig. 4b).DIC in the lower
295 layer was positively correlated with the Chl_L (Fig. 4) due to the abundant respiration in the lower
296 layer (Lin et al., 2021; Tsai et al., 2008).

298 **3.2 Performance of simulation data in conceptual two-layer DIC and DOC**
299 **models**

300 The results for the typhoon years demonstrated that that DIC_U was around 1.5 to 5.0
301 mg-C L⁻¹ (Fig. 5a–b) and DIC_L was around 5.0 mg-C L⁻¹ (Fig. 5d). In the non-typhoon years
302 (2017–2018), the NSE values of DIC_U and DIC_L were 0.61 and 0.70, respectively. On the other
303 hand, the DOC fit our observation data (R^2 values are 0.91, and 0.46; the NSE coefficients from
304 in equation (8) are 0.95 and 0.73) (Fig. 5c–d, Table 3). The parameters for the conceptual two-
305 layer DIC and DOC models showed different regimes between the typhoon and non-typhoon
306 years (Table 3). In the typhoon years, the photosynthesis absorption rate coefficients (α_{PU} , α_{PL})
307 were negative (photosynthesis < respiration) for each season. YYL was a C source due to a large
308 allochthonous C loading during typhoons; the respiration was elevated by around 30- to 150-fold
309 from summer to autumn. However, the values of the transportation coefficients (w_I) were higher
310 in autumn than in the other seasons (Table 3). Further, the higher remineralization rates during
311 typhoon disturbances from summer to autumn resulted in positive α_{MU} and α_{ML} . In the non-
312 typhoon years, the remineralization rates were negative (Table 3)..

313 We simulated the responses of DIC and DOC to typhoons using conceptual two-layer
314 C models. The results showed that the DIC was more sensitive to typhoon disturbances than
315 DOC under the scenarios of *Level 1* and *Level 2* (Fig. 5). Overall, the C level declined in the
316 upper layers but increased in the lower layers (Fig. 5). DIC and DOC in the upper layer tended
317 to decline from 1.0 (*Level 1*) to 2.0 mg-C L⁻¹ (*Level 2*) (Fig. 5a, c); however, they increased to
318 10.0 and 20.0 mg-C L⁻¹ in the lower layer under *Level 1* and *Level 2*, respectively (Fig. 5b, d).
319 Under extreme weather conditions, *Level 2* usually shifted to different typhoon responses for
320 each season (Fig. S1–S2) due to extreme river intrusions and strengths of thermal stratification
321 (Lin et al., 2021). DIC changes more than DOC under *Level 1* and *Level 2* (Fig. 5) because the
322 photosynthesis, transportation, and remineralization rates may crucially affect the seasonal and
323 interannual patterns of DOC as well.

325 3.3 *Interannual responses of NEP to typhoons under extreme weather scenarios*

326 We used filed observation data (Fig 5) to estimate the C fluxes in Table 4. The typhoon
327 disturbances in summer and autumn played an important role in promoting the C released by
328 YYL (Table 4). Overall, YYL released $245 \text{ mg C m}^{-3} \text{ d}^{-1}$ of DIC and $415 \text{ mg C m}^{-3} \text{ d}^{-1}$ of DOC
329 during the typhoon years; during the non-typhoon years, it released $51.7 \text{ mg C m}^{-3} \text{ d}^{-1}$ of DIC
330 and $22.8 \text{ mg C m}^{-3} \text{ d}^{-1}$ of DOC fluxes (Table 4). The average F_C was 219 and $133 \text{ mg C m}^{-3} \text{ d}^{-1}$
331 released from YYL into the atmosphere in the typhoon and non-typhoon years, respectively, one
332 to two times larger than Flux_{DIC} (Table 4). In summer, the upper layer exhibited declines in
333 both DIC and DOC concentrations, with DIC being approximately 3.7 times higher in DIC in
334 typhoons than in the non-typhoon years (Table 4). In autumn, 216 mg C d^{-1} of upper layer DIC
335 was released in the typhoon years, but $46.1 \text{ mg C m}^{-3} \text{ d}^{-1}$ of upper layer DOC was produced. The
336 upper layer Flux_{DIC} was negative in autumn in the typhoon years when $268 \text{ mg C m}^{-3} \text{ d}^{-1}$ more
337 F_C was released than in the non-typhoon years. In addition, the lower layer exhibited the largest
338 release of C into the outflow in the typhoon years; however, the flux in the lower layer was
339 more than twice as high in the summer as in the autumn of those years (Table 4). The average
340 total Flux_{DIC} was a release of approximately 3.14 times more C in the typhoon years than in the
341 non-typhoon years. The average total NEP_{DOC} showed an increase of $62.3 \text{ mg C m}^{-3} \text{ d}^{-1}$ of DOC
342 between the typhoon and non-typhoon years due to the over 10-fold higher flux in the upper
343 layer (Table 4).

344 We compared the fluxes with different model conditions (*Best-fit*, *Level 1*, and *Level*
345 2) as shown in Fig. 6, demonstrating that the responses of Flux_{DIC} to typhoons differed
346 dramatically between *Level 1* and *Level 2* (Fig. 6a-c); especially, the Upper Flux_{DIC} released
347 more C in the typhoon years and absorbed more C in the non-typhoon years than *Obs* (Fig. 6a).
348 Not only were the absolute values of Flux_{DIC} over 3 times higher in the typhoon years than in
349 the non-typhoon years (Table 4), but SD was higher in the typhoon years as well (Fig. 6).
350 However, DOC fluxes changed less under *Level 1* and *Level 2* (Fig. 6d-f), a finding that is
351 consistent with our continuous DOC data (Fig. 5c-d).

352 We not only attempted to know the contributions of thermal stratification and river
353 intrusion to DIC and DOC fluxes by using *Leve 1* and *Leve 2* scenarios in this conceptual model
354 but also the contributions of typhoon disturbances to DIC and DOC fluxes (Fig. 7). We found
355 the DIC and DOC fluxes were both released ($\Delta\text{Flux}_{\text{DIC}}$ and $\Delta\text{Flux}_{\text{DOC}}$) under *Leve 1* and *Leve*
356 2 scenarios (Fig. 7). Typhoon disturbances contributed -102.2 , $-62.3 \text{ mg-C m}^3 \text{ d}^{-1}$ Flux_{DIC} and
357 Flux_{DOC} in measurements (observation) data (*Obs*), respectively (Fig. 7). The averages of
358 $\Delta\text{Flux}_{\text{DIC}}$ under *Best-fit* was declined 7.0 % (*Leve 1*) and 30.0 % (*Leve 2*); $\Delta\text{Flux}_{\text{DOC}}$ was
359 declined 56.9 % (*Leve 1*) and 118 % (*Leve 2*), respectively (Fig. 7).

360 **4. Discussion**

361 **4.1 Biochemical and physical differences of DIC and DOC fluxes between**
362 **typhoon and non-typhoon-years in YYL**

363 The total precipitation was 35.6% higher in the typhoon years than in the non-typhoon
364 years (Table 1). Water retention and typhoon-induced upwelling control the dynamics of DIC
365 and DOC during the summer and autumn (Chiu et al., 2020; Jones et al., 2009; Tsai et al., 2008;
366 Tsai et al., 2011). The absence of typhoon-induced upwelling affected water quality data
367 differences between the upper and lower layers (Chiu et al., 2020; Lin et al., 2022; Tsai et al.,
368 2008; Tsai et al., 2011). DIC, DOC, and Chl. *a* concentrations differed significantly between
369 upper and lower layers in the non-typhoon years (Fig. 2). Further, the abundance of
370 microorganisms leads to intensive respirations in the lower layers during the non-typhoon
371 period in YYL; for example, an anoxic condition at the hypolimnion may decrease the
372 efficiency of C mineralization and remineralization rates in non-typhoon years (Carey et al.,
373 2022; Chiu et al., 2020; Lin et al., 2022; Shade et al., 2010; Shade et al., 2011). Thus, the
374 thermal stratification and anoxic condition may have been controlled by the seasonal and
375 interannual patterns of DIC and DOC fluxes in the non-typhoon years (Tables 3–4; Fig. 5).

376 We found positive correlations significantly between DOC and DIC concentrations in
377 typhoon years (Fig. 4) because substantial amounts of C loading into YYL during the strong
378 typhoon period in 2015 (Fig. 8a–b) due to the last drought year in 2014 (Chiu et al., 2020). Not
379 only the prolonged (or hysteresis) effects might lead to C emissions dramatically in 2015 due to
380 the drought year in 2014 (Chiu et al., 2020), but also the rapid water retention and C loading
381 during strong typhoon periods (Lin et al., 2022) induced vigorous algal biomass production in
382 the lower layer from May to September 2017 (Fig. 8d). Conversely, without the typhoon-
383 induced mixing and refreshing of the water column might be the mineralization dominated the
384 DIC and DOC concentrations in non-typhoon years (Chiu et al., 2020; Hanson et al., 2015; Lin
385 et al., 2022; Vachon et al., 2021), which could result in the positive linear relationship between
386 DIC and DOC concentrations (Fig. 4b, 8a), and negative remineralization rates in non-typhoon
387 years (Table 3). Therefore, these hydraulic, biogeochemical processes and the hysteresis effects
388 might describe different patterns of measurement data between the typhoon years and non-
389 typhoon years.

390 Thermal stratification and allochthonous C loading may drive the responses of fluxes
391 to typhoons in YYL. The absolute values of fluxes were higher in the typhoon years than in the
392 non-typhoon years (Table 4). We found that precipitation from typhoons loaded large amounts
393 of allochthonous C into YYL during summer and autumn, which might explain the higher fluxes
394 in autumn compared to the other seasons (Table 4). Typhoons dramatically changed the seasonal
395 and interannual patterns of DIC fluxes due to river intrusion (Fig. 5a–b; Fig. S1), which proves

396 to our hypothesis and corresponds to the results of previous studies (Chiu et al., 2020; Lin et al.,
397 2021; Lin et al., 2022). In summer, the DOC and DIC concentrations were spatial differences
398 between layers as a “two-layer system” within the water column because the upper and lower
399 layers were inhibited due to strong thermal stratification (Lin et al., 2021; Lin et al., 2022),
400 thereby resulted in the positive upper DIC and DOC fluxes and lower negative upper DIC and
401 DOC fluxes (Table 4).

402 Because of the absence of typhoon-induced mixing and allochthonous C loading, the
403 total fluxes were lower in the non-typhoon years than those in the typhoon years (Table 4). In
404 the typhoon years, our results showed that typhoon-induced upwelling and loading increased by
405 102.2 mg-DIC m⁻³ d⁻¹ and 62.3 mg-DOC m⁻³ d⁻¹ in YYL (Table 4). Additionally, the CO₂
406 emission (F_C) was 43 % higher (~83 mg C m⁻³ d⁻¹) in the typhoon years than in the non-typhoon
407 years (Table 4). Therefore, typhoon disturbances control DIC loading and C emissions in YYL,
408 consistent with our previous studies (Chiu et al., 2020; Lin et al., 2021; Lin et al., 2022).

409 Simultaneously, bio-photochemical mineralization and degradation may play a key role in
410 shaping C fluxes because colored DOC reduces ultraviolet radiation (UVR) and active
411 photosynthetic radiation (PAR) (Allesson et al., 2021; Chiu et al., 2020; Schindler et al., 1996;
412 Scully et al., 1996; Williamson et al., 1999), resulting in the higher light intensity and water
413 temperature in summer consuming 3.7 times more DIC and DOC than in the other seasons
414 (Table 4). These results suggested that the allochthonous C loading and light duration might be
415 the most crucial factor for DIC and DOC fluxes in the typhoon years. Conversely, the
416 transportation rate shaped the seasonal C concentrations due to thermal stratification in the non-
417 typhoon years.

419 4.2 ***Model limitation under the extreme weather scenarios***

420 Water temperature might be a crucial driver in controlling C fluxes in YYL (Chiu et
421 al., 2020; Lin et al., 2021; Lin et al., 2022). We found that the fluxes and F_{CO_2} in summer were
422 usually higher than in winter (Tables 3–4) due to the higher levels of photosynthesis,
423 remineralization, and thermal stratification strength (Lin et al., 2021; Lin et al., 2022). With the
424 conceptual two-layer C models (Table 3), photosynthesis absorption (α_{PU} , α_{PL}),
425 remineralization (α_{MU} , α_{ML}), and transportation (w_I) well represented the seasonal variations in
426 DIC and DOC data. These parameters of the conceptual two-layer C models appeared in
427 reasonable patterns (Table 3). The higher remineralization and photosynthesis rates resulted in
428 higher absolute values of fluxes in the autumn of the typhoon years (Tables 3–4). In the non-
429 typhoon years, the photosynthesis rates contributed to the total fluxes (Tables 3–4). Thus, the
430 conceptual two-layer C models well characterizes the seasonal and interannual responses of DIC
431 and DOC fluxes to typhoons in YYL.

432 Under the extreme weather events scenarios (*Level 1* and *Level 2*), the DIC and DOC
433 are more released 30 % –118 % within YYL, considering thermal stratification and river
434 intrusion. (Fig. 7). In non-typhoon years, the DIC fluxes were more absorbed than DOC fluxes
435 (Fig. 6) or events for each season (Fig. S1–S2) under extreme weather events scenarios.
436 However, the results showed that the typhoon disturbances that impacted the response of DOC
437 fluxes were more sensitive than DIC fluxes (Fig. 7). In autumn, our results are shown that
438 parameter of transportation rates in typhoon years was over ten-fold higher than non-typhoon
439 years (Table 3), but also DOC concentration was dominated by mineralization in typhoon years
440 (Fig. 8) because biogeochemical processes within lakes, such as respiration, mineralization, and
441 sediment burial, may impact DOC fluxes (Bartosiewicz et al., 2015; Hanson et al., 2015;
442 Maranger et al., 2018). Simultaneously, the physical processes such as typhoon-induced mixing
443 and fall overturns upwelled the sediment and lower layer DOC into the water surface in YYL
444 (Kimura et al. 2017; Lin et al. 2022). Therefore, we suggested that fall overturns and
445 mineralization after typhoon disturbances might be vital in the vertical distribution of DOC
446 concentrations in typhoon years.

447 Ejarque et al. (2021) successfully developed a conceptual one-layer model of DOC
448 and DIC, considering bacterial respiration, photo-mineralization and degradation in a temperate
449 mountain lake. In addition, Nagatomo et al. (2023) revealed the significance of “freshwater
450 carbon” that capture carbon due to photosynthesis and suggested that DIC might be
451 underestimated if submerged vegetation is ignored. We suggest that photo-biochemical
452 processes (such as photo-mineralization) and submerged vegetation should be considered in the
453 upper layer to clarify and validate the responses of the total C fluxes under extreme climates in a
454 two-layer stratified lake from the aspect of freshwater carbon ecosystem.

456 **5. Conclusions**

457 We successfully developed two-layer conceptual C models to obtain continuous DIC
458 and DOC data in YYL and to simulate extreme conditions. Our conceptual two-layer C model
459 revealed that allochthonous and autochthonous processes both accounted for C flux responses to
460 typhoon disturbances. Without typhoons, thermal stratification was the primary driver of
461 seasonal and interannual patterns of DIC and DOC. In the typhoon years, the changes in
462 seasonal river intrusion regimes in YYL resulted in a 3-fold higher total Flux_{DIC} than in the non-
463 typhoon years. However, our model should be improved for application to extreme climate
464 scenarios by considering other processes within lake, such as sediment burial, photo-
465 degradation processes, and anoxic conditions. The present results suggest that physical
466 processes (river intrusion and vertical transportation) and biogeochemical processes
467 (mineralization, photosynthesis, and respiration) in a subtropical small lake account for the C
468 flux responses to typhoons on seasonal and interannual time scales.

469

470 **Competing interests**

471 The authors have no conflicts of interest to report.

472

473 **Acknowledgements**

474 The authors thank YS Hsueh, LC Jiang, and TY Chen for their help with the water
475 sample collection and chemistry analysis. This work was supported by the Japan Society for the
476 Promotion of Science (JSPS) under grant nos. 22H05726, 22H01601, and 18KK0119 to K
477 Nakayama; and by the Academia Sinica, Taiwan (AS-103-TP-B15), Ministry of Science and
478 Technology, Taiwan (MOST 106-2621-M-239-001, MOST 107-2621-M-239-001, MOST 108-
479 2621-M-239-001) to CY Chiu and JW Tsai. This study benefited from participation in the
480 Global Lakes Ecological Observatory Network (GLEON).

481 Hao-Chi Lin: Conceptualization, Methodology, Investigation, Formal analysis,
482 Writing – original draft. Keisuke Nakayama: Methodology, Supervision, Writing – review &
483 editing, Conceptualization. Jeng-Wei Tsai: Investigation, Funding acquisition, Writing –review
484 & editing. Chih-Yu Chiu: Funding acquisition, Writing – review & editing.

485

486 **Data availability**

487 The data that support the findings of this study are adopted from our previous works,
488 including Chiu et al. (2020), Lin et al. (2021), and Lin et al. (2022). The DIC data
489 is available from <https://doi.org/10.5281/zenodo.3900032>, “The model outputs.

490

491

492 **References**

493 Allesson, L., Koehler, B., Thrane, J.-E., Andersen, T., and Hessen, D. O.: The role of
494 photomineralization for CO₂ emissions in boreal lakes along a gradient of dissolved organic
495 matter, *Limnol. Oceanogr.*, 66, 158–170, <https://doi.org/10.1002/lno.11594>, 2021.

496 Amaral, J. H. F., Melack, J. M., Barbosa, P. M., Borges, A. V., Kasper, D., Cortés, A. C., Zhou,
497 W., MacIntyre, S., and Forsberg, B. R.: Inundation, Hydrodynamics and Vegetation
498 Influence Carbon Dioxide Concentrations in Amazon Floodplain Lakes, *Ecosystems*, 25,
499 911–930, <https://doi.org/10.1007/s10021-021-00692-y>, 2022.

500 Aufdenkampe, A. K., Mayorga, E., Raymond, P. A., Melack, J. M., Doney, S. C., Alin, S. R.,
501 Aalto, R. E., and Yoo, K.: Riverine coupling of biogeochemical cycles between land,
502 oceans, and atmosphere, *Front. Ecol. Environ.*, 9, 53–60, <https://doi.org/10.1890/100014>,
503 2011.

504 Bartosiewicz, M., Laurion, I., and MacIntyre, S.: Greenhouse gas emission and storage in a
505 small shallow lake, *Hydrobiologia*, 757, 101–115, <https://doi.org/10.1007/s10750-015-2240-2>, 2015.

506 Cai, W.-J. and Wang, Y.: The chemistry, fluxes, and sources of carbon dioxide in the estuarine
507 waters of the Satilla and Altamaha Rivers, Georgia, *Limnol. Oceanogr.*, 43, 657–668,
508 <https://doi.org/10.4319/lo.1998.43.4.0657>, 1998.

509 Carey, C. C., Hanson, P. C., Thomas, R. Q., Gerling, A. B., Hounshell, A. G., Lewis, A. S. L.,
510 Lofton, M. E., McClure, R. P., Wander, H. L., Woelmer, W. M., Niederlehner, B. R., and
511 Schreiber, M. E.: Anoxia decreases the magnitude of the carbon, nitrogen, and phosphorus
512 sink in freshwaters, *Glob. Change Biol.*, <https://doi.org/10.1111/gcb.16228>, 2022.

513 Chang, S.-C., Wang, C.-P., Feng, C.-M., Rees, R., Hell, U., and Matzner, E.: Soil fluxes of
514 mineral elements and dissolved organic matter following manipulation of leaf litter input in
515 a Taiwan Chamaecyparis forest, *For. Ecol. Manag.*, 242, 133–141,
516 <https://doi.org/10.1016/j.foreco.2007.01.025>, 2007.

517 Chiu, C.-Y., Jones, J. R., Rusak, J. A., Lin, H.-C., Nakayama, K., Kratz, T. K., Liu, W.-C., Tang,
518 S.-L., and Tsai, J.-W.: Terrestrial loads of dissolved organic matter drive inter-annual carbon
519 flux in subtropical lakes during times of drought, *Sci. Total Environ.*, 717, 137052,
520 <https://doi.org/10.1016/j.scitotenv.2020.137052>, 2020.

521 Chou, C.-H., Chen, T.-Y., Liao, C.-C., and Peng, C.-I.: Long-term ecological research in the
522 Yuanyang Lake forest ecosystem I. Vegetation composition and analysis, *Bot. Bull. Acad.
523 Sin.*, 41, 61–72, 2000.

524 Cole, J. J. and Caraco, N. F.: Atmospheric exchange of carbon dioxide in a low-wind

526 oligotrophic lake measured by the addition of SF₆, Limnol. Oceanogr., 43, 647–656,
527 <https://doi.org/10.4319/lo.1998.43.4.0647>, 1998.

528 Cole, J. J., Prairie, Y. T., Caraco, N. F., McDowell, W. H., Tranvik, L. J., Striegl, R. G., Duarte,
529 C. M., Kortelainen, P., Downing, J. A., Middelburg, J. J., and Melack, J.: Plumbing the
530 Global Carbon Cycle: Integrating Inland Waters into the Terrestrial Carbon Budget,
531 Ecosystems, 10, 172–185, <https://doi.org/10.1007/s10021-006-9013-8>, 2007.

532 Czikowsky, M. J., MacIntyre, S., Tedford, E. W., Vidal, J., and Miller, S. D.: Effects of Wind
533 and Buoyancy on Carbon Dioxide Distribution and Air-Water Flux of a Stratified Temperate
534 Lake, J. Geophys. Res. Biogeosci., 123, 2305–2322, <https://doi.org/10.1029/2017JG004209>,
535 2018.

536 Dodds, W. K. and Whiles, M. R.: Freshwater Ecology: Concepts and Environmental
537 Applications of Limnology, Third Edition, Elsevier, United Kingdom, 748-762, 2020.

538 Doubek, J. P., Anneville, O., Dur, G., Lewandowska, A. M., Patil, V. P., Rusak, J. A., Salmaso,
539 N., Seltmann, C. T., Straile, D., Urrutia-Cordero, P., Venail, P., Adrian, R., Alfonso, M. B.,
540 DeGasperi, C. L., Eyto, E., Feuchtmayr, H., Gaiser, E. E., Girdner, S. F., Graham, J. L.,
541 Grossart, H.-P., Hejzlar, J., Jacquet, S., Kirillin, G., Llames, M. E., Matsuzaki, S.-I. S.,
542 Nodine, E. R., Piccolo, M. C., Pierson, D. C., Rimmer, A., Rudstam, L. G., Sadro, S., Swain,
543 H. M., Thackeray, S. J., Thiery, W., Verburg, P., Zohary, T., and Stockwell, J. D.: The extent
544 and variability of storm-induced temperature changes in lakes measured with long-term and
545 high-frequency data, Limnol. Oceanogr., 66, 1979–1992, <https://doi.org/10.1002/lno.11739>,
546 2021.

547 Douville, H., Raghavan, K., Renwick, J., Allan, R. P., Arias, P. A., Barlow, M., Cerezo-Mota, R.,
548 Cherchi, A., Gan, T. Y., Gergis, J., Jiang, D., Khan, A., Mba, W. P., Rosenfeld, D., Tierney,
549 J., and Zolina, O.: Water cycle changes, Cambridge University Press, Climate Change 2021:
550 The Physical Science Basis. Contribution of Working Group I to 45 the Sixth Assessment
551 Report of the Intergovernmental Panel on Climate Change, 2021.

552 Downing, J. A., Prairie, Y. T., Cole, J. J., Duarte, C. M., Tranvik, L. J., Striegl, R. G.,
553 McDowell, W. H., Kortelainen, P., Caraco, N. F., Melack, J. M., and Middelburg, J. J.: The
554 global abundance and size distribution of lakes, ponds, and impoundments, Limnol.
555 Oceanogr., 51, 2388–2397, <https://doi.org/10.4319/lo.2006.51.5.2388>, 2006.

556 Ejarque, E., Scholz, K., Wohlfahrt, G., Battin, T. J., Kainz, M. J., and Schelker, J.: Hydrology
557 controls the carbon mass balance of a mountain lake in the eastern European Alps, Limnol.
558 Oceanogr., 66, 2110–2125, <https://doi.org/10.1002/lno.11712>, 2021.

559 Engel, F., Farrell, K. J., McCullough, I. M., Scordo, F., Denfeld, B. A., Dugan, H. A., Eyto, E.
560 de, Hanson, P. C., McClure, R. P., Nõges, P., Nõges, T., Ryder, E., Weathers, K. C., and
561 Weyhenmeyer, G. A.: A lake classification concept for a more accurate global estimate of

562 the dissolved inorganic carbon export from terrestrial ecosystems to inland waters, *Sci. Nat.*,
563 105, 25, <https://doi.org/10.1007/s00114-018-1547-z>, 2018.

564 Hanson, P. C., Pace, M. L., Carpenter, S. R., Cole, J. J., and Stanley, E. H.: Integrating
565 Landscape Carbon Cycling: Research Needs for Resolving Organic Carbon Budgets of
566 Lakes, *Ecosystems*, 18, 363–375, <https://doi.org/10.1007/s10021-014-9826-9>, 2015.

567 Hope, D., Palmer, S. M., Billett, M. F., and Dawson, J. J. C.: Variations in dissolved CO₂ and
568 CH₄ in a first-order stream and catchment: an investigation of soil-stream linkages, *Hydrol.*
569 *Process.*, 18, 3255–3275, <https://doi.org/10.1002/hyp.5657>, 2004.

570 Jähne, B., Münnich, K. O., Bösinger, R., Dutzi, A., Huber, W., and Libner, P.: On the parameters
571 influencing air-water gas exchange, *J. Geophys. Res. Oceans*, 92, 1937,
572 <https://doi.org/10.1029/JC092iC02p01937>, 1987.

573 Jones, S. E., Kratz, T. K., Chiu, C.-Y., and McMahon, K. D.: Influence of typhoons on annual
574 CO₂ flux from a subtropical, humic lake, *Glob. Change Biol.*, 15, 243–254,
575 <https://doi.org/10.1111/j.1365-2486.2008.01723.x>, 2009.

576 Kimura, N., Liu, W.-C., Chiu, C.-Y., and Kratz, T.: The influences of typhoon-induced mixing in
577 a shallow lake, *Lakes Reserv.: Res. Manag.*, 17, 171–183, <https://doi.org/10.1111/j.1440-1770.2012.00509.x>, 2012.

578 Kimura, N., Liu, W.-C., Tsai, J.-W., Chiu, C.-Y., Kratz, T. K., and Tai, A.: Contribution of
579 extreme meteorological forcing to vertical mixing in a small, shallow subtropical lake, *J.*
580 *Limnol.*, 76, 116–128, <https://doi.org/10.4081/jlimnol.2016.1477>, 2017.

581 Kossin, J. P., Olander, T. L., and Knapp, K. R.: Trend Analysis with a New Global Record of
582 Tropical Cyclone Intensity, *J. Clim.*, 26, 9960–9976, <https://doi.org/10.1175/JCLI-D-13-00262.1>, 2013.

583 Kraemer, B. M., Pilla, R. M., Woolway, R. I., Anneville, O., Ban, S., Colom-Montero, W.,
584 Devlin, S. P., Dokulil, M. T., Gaiser, E. E., Hambright, K. D., Hessen, D. O., Higgins, S. N.,
585 Jöhnk, K. D., Keller, W., Knoll, L. B., Leavitt, P. R., Lepori, F., Luger, M. S., Maberly, S. C.,
586 Müller-Navarra, D. C., Paterson, A. M., Pierson, D. C., Richardson, D. C., Rogora, M.,
587 Rusak, J. A., Sadro, S., Salmaso, N., Schmid, M., Silow, E. A., Sommaruga, R., Stelzer, J. A.
588 A., Straile, D., Thiery, W., Timofeyev, M. A., Verburg, P., Weyhenmeyer, G. A., and Adrian,
589 R.: Climate change drives widespread shifts in lake thermal habitat, *Nat. Clim. Chang.*, 11,
590 521–529, <https://doi.org/10.1038/s41558-021-01060-3>, 2021.

591 Lai, I.-L., Chang, S.-C., Lin, P.-H., Chou, C.-H., and Wu, J.-T.: Climatic Characteristics of the
592 Subtropical Mountainous Cloud Forest at the Yuanyang Lake Long-Term Ecological
593 Research Site, Taiwan, *Taiwania*, 51, 317–329, 2006.

594 Lauerwald, R., Laruelle, G. G., Hartmann, J., Ciais, P., and Regnier, P. A.: Spatial patterns in
595 CO₂ evasion from the global river network, *Global Biogeochem. Cycles*, 29, 534–554,

598 <https://doi.org/10.1002/2014GB004941>, 2015.

599 Lin, H.-C., Chiu, C.-Y., Tsai, J.-W., Liu, W.-C., Tada, K., and Nakayama, K.: Influence of
600 Thermal Stratification on Seasonal Net Ecosystem Production and Dissolved Inorganic
601 Carbon in a Shallow Subtropical Lake, *J. Geophys. Res. Biogeosci.*, 126,
602 <https://doi.org/10.1029/2020JG005907>, 2021.

603 Lin, H.-C., Tsai, J.-W., Tada, K., Matsumoto, H., Chiu, C.-Y., and Nakayama, K.: The impacts
604 of the hydraulic retention effect and typhoon disturbance on the carbon flux in shallow
605 subtropical mountain lakes, *Sci. Total Environ.*, 803, 150044,
606 <https://doi.org/10.1016/j.scitotenv.2021.150044>, 2022.

607 Maberly, S. C., O'Donnell, R. A., Woolway, R. I., Cutler, M. E. J., Gong, M., Jones, I. D.,
608 Merchant, C. J., Miller, C. A., Politi, E., Scott, E. M., Thackeray, S. J., and Tyler, A. N.:
609 Global lake thermal regions shift under climate change, *Nat Commun.*, 11, 1232,
610 <https://doi.org/10.1038/s41467-020-15108-z>, 2020.

611 MacIntyre, S., Bastviken, D., Arneborg, L., Crowe, A. T., Karlsson, J., Andersson, A., Gålfalk,
612 M., Rutgersson, A., Podgrajsek, E., and Melack, J. M.: Turbulence in a small boreal lake:
613 Consequences for air-water gas exchange, *Limnol. Oceanogr.*, 66, 827–854,
614 <https://doi.org/10.1002/lno.11645>, 2021.

615 Maranger, R., Jones, S. E., and Cotner, J. B.: Stoichiometry of carbon, nitrogen, and phosphorus
616 through the freshwater pipe, *Limnol Oceanogr Lett*, 3, 89–101,
617 <https://doi.org/10.1002/lol2.10080>, 2018.

618 Marcé, R., Obrador, B., Gómez-Gener, L., Catalán, N., Koschorreck, M., Arce, M. I., Singer, G.,
619 and Schiller, D. von: Emissions from dry inland waters are a blind spot in the global carbon
620 cycle, *Earth-Sci. Rev.*, 188, 240–248, <https://doi.org/10.1016/j.earscirev.2018.11.012>, 2019.

621 Nagatomo, K., Nakayama, K., Komai, K., Matsumoto, H., Watanabe, K., Kubo, A., Tada, K.,
622 Maruya, Y., Yano, S., Tsai, J. W., Lin, H. C., Vilas, M., and Hipsey, M. R.: A Spatially
623 Integrated Dissolved Inorganic Carbon (SiDIC) Model for Aquatic Ecosystems Considering
624 Submerged Vegetation, *J Geophys Res Biogeosci*, 128,
625 <https://doi.org/10.1029/2022JG007032>, 2023.

626 Nakayama, K., Kawahara, Y., Kurimoto, Y., Tada, K., Lin, H.-C., Hung, M.-C., Hsueh, M.-L.,
627 and Tsai, J.-W.: Effects of oyster aquaculture on carbon capture and removal in a tropical
628 mangrove lagoon in southwestern Taiwan, *Sci. Total Environ.*, 156460,
629 <https://doi.org/10.1016/j.scitotenv.2022.156460>, 2022.

630 Nakayama, K., Komai, K., Tada, K., Lin, H. C., Yajima, H., Yano, S., Hipsey, M. R., and Tsai, J.
631 W.: Modeling dissolved inorganic carbon considering submerged aquatic vegetation, *Ecol.
632 Model.*, 431, 109188, <https://doi.org/10.1016/j.ecolmodel.2020.109188>, 2020.

633 Nakayama, K., Sivapalan, M., Sato, C., and Furukawa, K.: Stochastic characterization of the

634 onset of and recovery from hypoxia in Tokyo Bay, Japan: Derived distribution analysis
635 based on “strong wind” events, *Water Resour. Res.*, 46,
636 <https://doi.org/10.1029/2009WR008900>, 2010.

637 Nash, J. E. and Sutcliffe, J. V.: River flow forecasting through conceptual models, I A discussion
638 of principles, *J. Hydrol.*, 10, 398–409, 1970.

639 Olsson, F., Mackay, E. B., Barker, P., Davies, S., Hall, R., Spears, B., Exley, G., Thackeray, S.
640 J., and Jones, I. D.: Can reductions in water residence time be used to disrupt seasonal
641 stratification and control internal loading in a eutrophic monomictic lake?, *J. Environ.*
642 *Manage.*, 304, 114169, <https://doi.org/10.1016/j.jenvman.2021.114169>, 2022a.

643 Olsson, F., Mackay, E. B., Moore, T., Barker, P., Davies, S., Hall, R., Spears, B., Wilkinson, J.,
644 and Jones, I. D.: Annual water residence time effects on thermal structure: A potential lake
645 restoration measure?, *J. Environ. Manage.*, 314, 115082,
646 <https://doi.org/10.1016/j.jenvman.2022.115082>, 2022b.

647 Plummer, L. and Busenberg, E.: The solubilities of calcite, aragonite and vaterite in $\text{CO}_2\text{-H}_2\text{O}$
648 solutions between 0 and 90°C, and an evaluation of the aqueous model for the system
649 $\text{CaCO}_3\text{-CO}_2\text{-H}_2\text{O}$, *Geochim. Cosmochim. Acta*, 46, 1011–1040,
650 [https://doi.org/10.1016/0016-7037\(82\)90056-4](https://doi.org/10.1016/0016-7037(82)90056-4), 1982.

651 Raymond, P. A., Hartmann, J., Lauerwald, R., Sobek, S., McDonald, C., Hoover, M., Butman,
652 D., Striegl, R., Mayorga, E., Humborg, C., Kortelainen, P., Dürr, H., Meybeck, M., Ciais, P.,
653 and Guth, P.: Global carbon dioxide emissions from inland waters, *Nature*, 503, 355–359,
654 <https://doi.org/10.1038/nature12760>, 2013.

655 Schindler, D. W., Curtis, P. J., Parker, B. R., and Stainton, M. P.: Consequences of climate
656 warming and lake acidification for UV-B penetration in North American boreal lakes,
657 *Nature*, 379, 705–708, <https://doi.org/10.1038/379705a0>, 1996.

658 Scully, N. M., McQueen, D. J., and Lean, D. R. S.: Hydrogen peroxide formation: The
659 interaction of ultraviolet radiation and dissolved organic carbon in lake waters along a 43–
660 75°N gradient, *Limnol. Oceanogr.*, 41, 540–548, <https://doi.org/10.4319/lo.1996.41.3.0540>,
661 1996.

662 Shade, A., Chiu, C.-Y., and McMahon, K. D.: Seasonal and episodic lake mixing stimulate
663 differential planktonic bacterial dynamics, *Microb. Ecol.*, 59, 546–554,
664 <https://doi.org/10.1007/s00248-009-9589-6>, 2010.

665 Shade, A., Read, J. S., Welkie, D. G., Kratz, T. K., Wu, C. H., and McMahon, K. D.: Resistance,
666 resilience and recovery: aquatic bacterial dynamics after water column disturbance, *Environ.*
667 *Microbiol.*, 13, 2752–2767, <https://doi.org/10.1111/j.1462-2920.2011.02546.x>, 2011.

668 Shih, Y.-T., Chen, P.-H., Lee, L.-C., Liao, C.-S., Jien, S.-H., Shiah, F.-K., Lee, T.-Y., Hein, T.,
669 Zehetner, F., Chang, C.-T., and Huang, J.-C.: Dynamic responses of DOC and DIC transport

670 to different flow regimes in a subtropical small mountainous river, *Hydrol. Earth Syst. Sci.*,
671 22, 6579–6590, <https://doi.org/10.5194/hess-22-6579-2018>, 2019.

672 Smith, S. V.: Physical, chemical and biological characteristics* of CO₂ gas flux across the air-
673 water interface, *Plant Cell Environ.*, 8, 387–398, <https://doi.org/10.1111/j.1365->
674 3040.1985.tb01674.x, 1985.

675 Sobek, S., Tranvik, L. J., and Cole, J. J.: Temperature independence of carbon dioxide
676 supersaturation in global lakes, *Global Biogeochem. Cycles*, 19, GB2003,
677 <https://doi.org/10.1029/2004GB002264>, 2005.

678 Sun, P., He, S., Yu, S., Pu, J., Yuan, Y., and Zhang, C.: Dynamics in riverine inorganic and
679 organic carbon based on carbonate weathering coupled with aquatic photosynthesis in a
680 karst catchment, *Southwest China, Water Research*, 189, 116658,
681 <https://doi.org/10.1016/j.watres.2020.116658>, 2021.

682 Tranvik, L. J., Downing, J. A., Cotner, J. B., Loiselle, S. A., Striegl, R. G., Ballatore, T. J.,
683 Dillon, P., Finlay, K., Fortino, K., Knoll, L. B., Kortelainen, P. L., Kutser, T., Larsen, S.,
684 Laurion, I., Leech, D. M., McCallister, S. L., McKnight, D. M., Melack, J. M., Overholt, E.,
685 Porter, J. A., Prairie, Y., Renwick, W. H., Roland, F., Sherman, B. S., Schindler, D. W.,
686 Sobek, S., Tremblay, A., Vanni, M. J., Verschoor, A. M., Wachenfeldt, E. von, and
687 Weyhenmeyer, G. A.: Lakes and reservoirs as regulators of carbon cycling and climate,
688 *Limnol. Oceanogr.*, 54, 2298–2314, https://doi.org/10.4319/lo.2009.54.6_part_2.2298, 2009.

689 Tsai, J.-W., Kratz, T. K., Hanson, P. C., Kimura, N., Liu, W.-C., Lin, F.-P., Chou, H.-M., Wu, J.-
690 T., and Chiu, C.-Y.: Metabolic changes and the resistance and resilience of a subtropical
691 heterotrophic lake to typhoon disturbance, *Can. J. Fish. Aquat. Sci.*, 68, 768–780,
692 <https://doi.org/10.1139/F2011-024>, 2011.

693 Tsai, J.-W., Kratz, T. K., Hanson, P. C., Wu, J.-T., Chang, W. Y. B., Arzberger, P. W., Lin, B.-S.,
694 Lin, F.-P., Chou, H.-M., and Chiu, C.-Y.: Seasonal dynamics, typhoons and the regulation of
695 lake metabolism in a subtropical humic lake, *Freshw. Biol.*, 53, 1929–1941,
696 <https://doi.org/10.1111/j.1365-2427.2008.02017.x>, 2008.

697 Vachon, D. and Del Giorgio, P. A.: Whole-Lake CO₂ Dynamics in Response to Storm Events in
698 Two Morphologically Different Lakes, *Ecosystems*, 17, 1338–1353,
699 <https://doi.org/10.1007/s10021-014-9799-8>, 2014.

700 Vachon, D., Sponseller, R. A., and Karlsson, J.: Integrating carbon emission, accumulation and
701 transport in inland waters to understand their role in the global carbon cycle, *Glob. Change
702 Biol.*, 27, 719–727, <https://doi.org/10.1111/gcb.15448>, 2021.

703 Wanninkhof, R.: Relationship between wind speed and gas exchange over the ocean, *J.
704 Geophys. Res. Oceans*, 97, 7373, <https://doi.org/10.1029/92JC00188>, 1992.

705 Williamson, C. E., Morris, D. P., Pace, M. L., and Olson, O. G.: Dissolved organic carbon and

706 nutrients as regulators of lake ecosystems: Resurrection of a more integrated paradigm,
707 Limnol. Oceanogr., 44, 795–803, https://doi.org/10.4319/lo.1999.44.3_part_2.0795, 1999.

708 Winslow, L. A., Read, J. S., Hansen, G. J. A., and Hanson, P. C.: Small lakes show muted
709 climate change signal in deepwater temperatures, Geophys. Res. Lett., 42, 355–361,
710 <https://doi.org/10.1002/2014GL062325>, 2015.

711 Woolway, R. I., Anderson, E. J., and Albergel, C.: Rapidly expanding lake heatwaves under
712 climate change, Environ. Res. Lett., 16, 94013, <https://doi.org/10.1088/1748-9326/ac1a3a>,
713 2021a.

714 Woolway, R. I., Jennings, E., Shatwell, T., Golub, M., Pierson, D. C., and Maberly, S. C.: Lake
715 heatwaves under climate change, Nature, 589, 402–407, <https://doi.org/10.1038/s41586-020-03119-1>, 2021b.

717 Woolway, R. I., Kraemer, B. M., Lengers, J. D., Merchant, C. J., O'Reilly, C. M., and Sharma, S.:
718 Global lake responses to climate change, Nat. Rev. Earth Environ., 1, 388–403,
719 <https://doi.org/10.1038/s43017-020-0067-5>, 2020.

720 Woolway, R. I., Simpson, J. H., Spiby, D., Feuchtmayr, H., Powell, B., and Maberly, S. C.: Physical
721 and chemical impacts of a major storm on a temperate lake: a taste of things to come?, Climatic
722 Change, 151, 333–347, <https://doi.org/10.1007/s10584-018-2302-3>, 2018.

723 Wu, J.-T., Chang, S.-C., Wang, Y.-S., and Hsu, M.-K.: Characteristics of the acidic environment of
724 the Yuanyang Lake (Taiwan), Bot. Bull. Acad. Sin., 42, 17–22, 2001.

725 Zhou, Y., Yu, X., Zhou, L., Zhang, Y., Xu, H., Zhu, M., Zhu, G., Jang, K.-S., Spencer, R. G. M.,
726 Jeppesen, E., Brookes, J. D., Kothawala, D. N., and Wu, F.: Rainstorms drive export of aromatic
727 and concurrent bio-labile organic matter to a large eutrophic lake and its major tributaries, Water
728 Research, 229, 119448, <https://doi.org/10.1016/j.watres.2022.119448>, 2023.

729 Zwart, J. A., Sebestyen, S. D., Solomon, C. T., and Jones, S. E.: The Influence of Hydrologic
730 Residence Time on Lake Carbon Cycling Dynamics Following Extreme Precipitation Events,
731 Ecosystems, 20, 1000–1014, <https://doi.org/10.1007/s10021-016-0088-6>, 2017.

732

733 **Table 1.** Comparison of Yuan-Yang Lake's rainfall and hydrological records in typhoon and non-
734 typhoon years.

Records	Typhoon years	Non-typhoon years
Time period (year)	2015-2016	2017-2018
Total precipitation (mm)	6,332	3,795
Total typhoon rainfall (mm)	2,254	0
Annual average wind speed (m s^{-1})	1.20	1.11
Average water depth ($\text{m} \pm \text{SD}$)	4.54 ± 1.7	4.51 ± 1.5
Average river discharge ($\text{m}^3 \text{ d}^{-1}$)	3,717	2,943
Transparency (Secchi disc depth, $\text{m} \pm \text{SD}$)	1.58 ± 0.45	1.38 ± 0.28

735

Table 2. Parameters of the two-layer conceptual model in Yuan-Yang Lake

Parameters	Value	Unit
<u>Measurements</u>		
Q_{out}	Outflow discharge	Daily data
Q_{in}	Inflow discharge	Daily data
Q_U	Upper layer discharge	Daily data
Q_L	Lower layer discharge	Daily data
DIC_R	River inflow DIC	Monthly data
DIC_U	Upper layer DIC	Monthly data
DIC_L	Lower layer DIC	Monthly data
Chl_U	Upper layer Chl a	Monthly data
Chl_L	Lower layer Chl a	Monthly data
DOC_U	Upper layer DOC	Monthly data
DOC_L	Lower layer DOC	Monthly data
F_{CO_2}	Carbon emission (equation 7)	Monthly data
<u>Constants</u>		
V_{total}	Total lake volume	m^3
V_U	Upper layer volume	m^3
V_L	Lower layer volume	m^3
A_s	Lake surface area	m^2
A_I	Interface area	m^2
A_B	Bottom of lake area	m^2
C_U	Coefficient of the standard unit	$L m^{-3}$
<u>Unknown Constants</u>		
α_{PU}, α_{PL}	Coefficients of photosynthesis	Constant
α_{MU}, α_{ML}	Coefficients of mineralization	Constant
w_I	Coefficient of vertical transportation	Constant
BF_{DIC}, BF_{DOC}	Sediment DIC and DOC emission	Constant
Pa_U, Pb_L	Equations constant at lower layer	Constant
<u>Extreme scenarios</u>		
<i>Best-fit</i>	Q_U	Q_L
	75% (spring), Q_U and Q_L are followed buoyancy frequency for each season (Lin et al. 2021)	25% (spring), 80% (summer), 45% (autumn), 50% (winter) of Q_{in}
<i>of Q_{in}</i>		

<i>Level 1</i>	Best-fit scenario but change upper- and lower-layers discharges (Q_U, Q_L)	77% (spring), 82% (summer), 47% (autumn), 50% (winter)	23% (spring), 18% (summer), 53% (autumn), 50% (winter)
<i>Level 2</i>	Best-fit scenario but change upper- and lower layers discharges (Q_U, Q_L)	of Q_{in} 80% (spring), 85% (summer), 50% (autumn), 50% (winter)	of Q_{in} . 20% (spring), 15% (summer), 50% (autumn), 50% (winter)

738 **Table 3.** Best-fit parameters of a two-layer conceptual model of DIC and DOC in Yuan-Yang
 739 Lake from 2015 to 2018.

	2015–2016				2017–2018			
	Typhoon years				Non-typhoon years			
	Spring	Summer	Autumn	Winter	Spring	Summer	Autumn	Winter
<u>Upper layer</u>								
F_{CO_2} (mg-C m ² d ⁻¹)	291	245	422	127	231	143	104	175
α_{PU} (d ⁻¹)	-1.20	-33.1	-183.5	-29.1	8.0	6.0	30.0	7.77
α_{MU} (d ⁻¹)	-0.0227	0.0203	0.08	-0.031	-0.01	-0.039	-0.033	-0.195
w_I (d ⁻¹)	0.230	0.172	1.38	0.30	0.10	0.0478	0.120	0.180
Pa_U (d ⁻¹)	12560	-1317	-23750	9597	9880	14000	17600	10100
Pb_U (d ⁻¹)	-21930	9461	-42130	-17070	-3630	-1251	-20820	-9289
$dDIC_U$ (R ² , NSE)					0.305, 0.614			
$dDOC_U$ (R ² , NSE)					0.909, 0.953			
<u>Lower layer</u>								
α_{PL} (d ⁻¹)	-0.627	-22.1	15.0	-0.878	1.49	-6.87	6.0	-16.6
α_{ML} (d ⁻¹)	-0.025	0.123	0.0755	0.00973	-0.010	-0.0376	-0.04	-0.048
Pa_L (d ⁻¹)	100	-5662	-10500	-1013	151.6	2032	1216	909
Pb_L (d ⁻¹)	-6012	-7395	-53940	-9639	-1338	-6296	-19470	-8748
BF_{DIC} , BF_{DOC} (mg-C L ⁻¹)					0.04,			
					0.00			
$dDIC_L$ (R ² , NSE)					0.452, 0.707			
$dDOC_L$ (R ² , NSE)					0.460, 0.728			

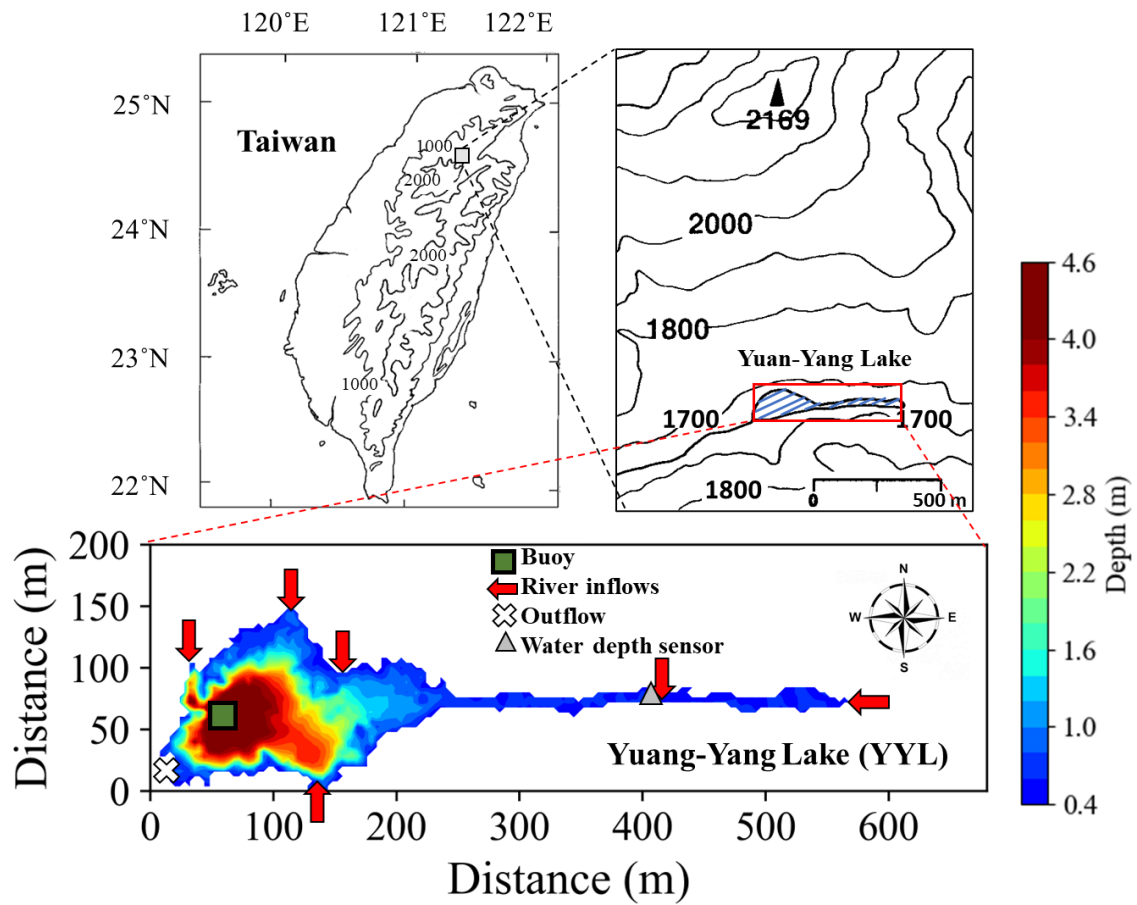
740

741 **Table 4.** Seasonal averages of carbon fluxes ($\text{mg C m}^{-3} \text{ d}^{-1}$) for each season in Yuan-Yang Lake.
 742 Positive values are shown in the carbon sink, and negative ones show the values after carbon was
 743 released. F_C was carbon emission across water to air by using empirical equations method (Lin
 744 et al.2021).

		Flux			Total	
		F_C	Upper	Lower	Flux_{DIC}	Flux_{DOC}
<i>Typhoon years</i>	Average	-219	-	-	-150	-9.69
Spring	DIC	-231	-243	-45.2	-210	62.1
	DOC	-	70.8	17.2		
Summer	DIC	-194	29.1	-313	-26.4	18.8
	DOC	-	118	-495		
Autumn	DIC	-351	-216	-659	-288	-151
	DOC	-	46.1	-1167		
Winter	DIC	-100	-96.4	36.5	-74.8	31.2
	DOC	-	40.5	-16.9		
<i>Non-typhoon years</i>	Average	-133	-	-	-47.8	52.6
Spring	DIC	-129	-180	-94.9	-166	-7.06
	DOC	-	21.4	-67.1		
Summer	DIC	-183	5.80	-58.1	-4.57	73.8
	DOC	-	115	-140		
Autumn	DIC	-82.6	95.0	35.9	85.5	95.9
	DOC	-	168	-272		
Winter	DIC	-138	-128	6.04	-106	33.7
	DOC	-	34.0	32.1		

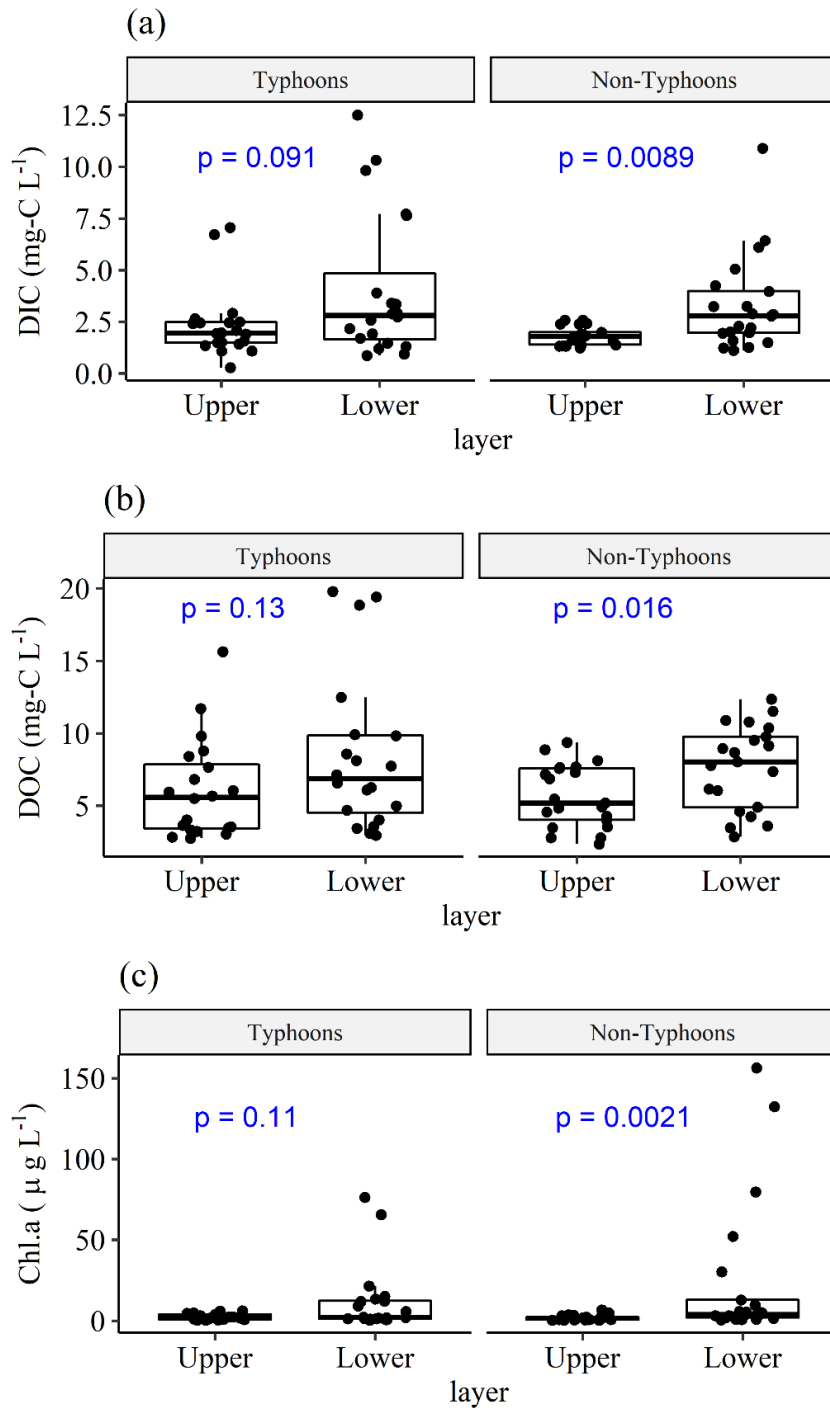
745

746

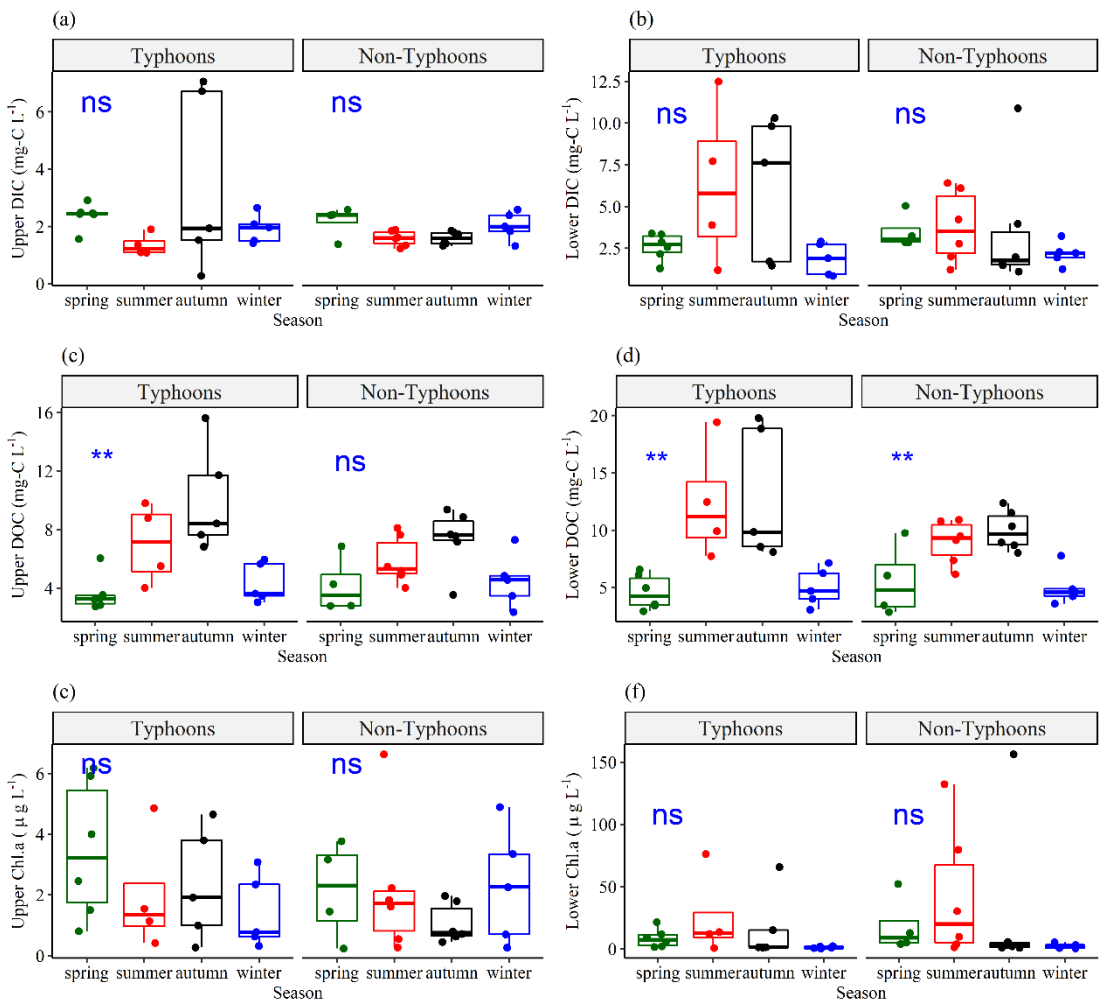


747

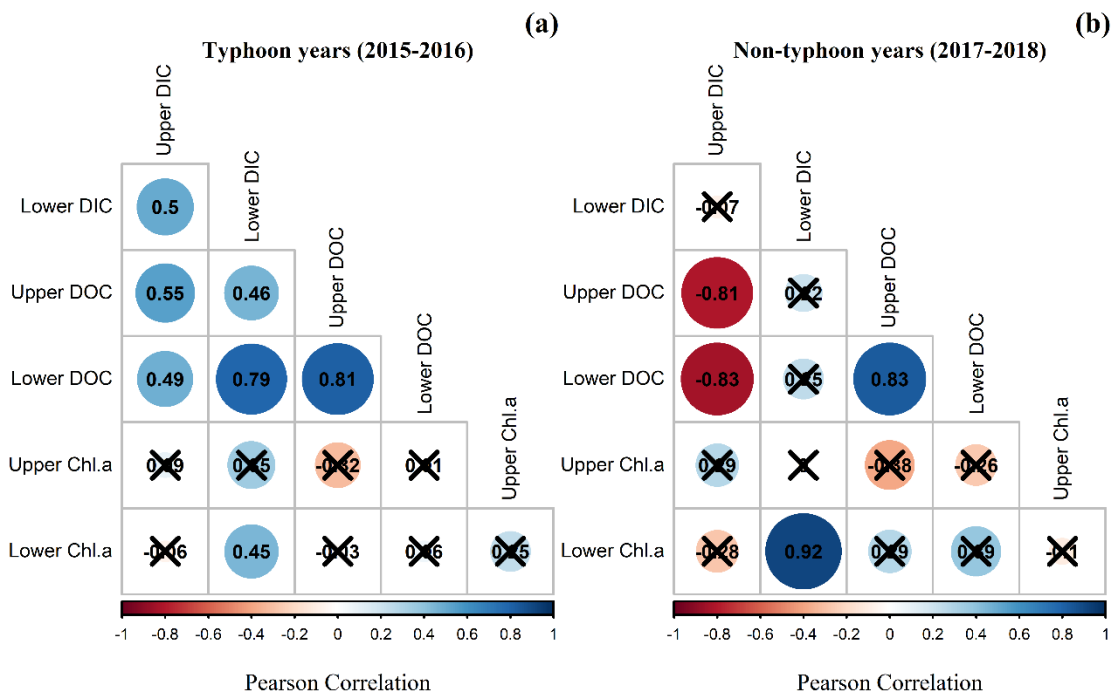
748 **Fig. 1.** Sampling locations and bathymetry maps of Yuan-Yang Lake (YYL). The dark
749 rectangle shows the buoy station, which is located at the deepest site of the lake.
750 The *red points* and *white cross* show the river mouths of the inflows and outflows,
751 respectively. The *gray triangle* shows the location of the water depth sensor.
752



753
754 **Fig. 2.** Comparisons of (a) DIC, (b) DOC, and (c) Chl *a* between upper (DIC_U , DOC_U ,
755 Chl_U) and lower (DIC_L , DOC_L , Chl_L) layers, grouped by typhoon and non-typhoon
756 years. *Bullet points* show the water sampling data. We used a t-test to obtain the *p*-
757 values (blue texts). Total sampling numbers are 41 ($n = 41$) for each measurement from
758 January 2015 to December 2018; $n = 20$ in typhoon years, and $n = 21$ in non-typhoon
759 years.



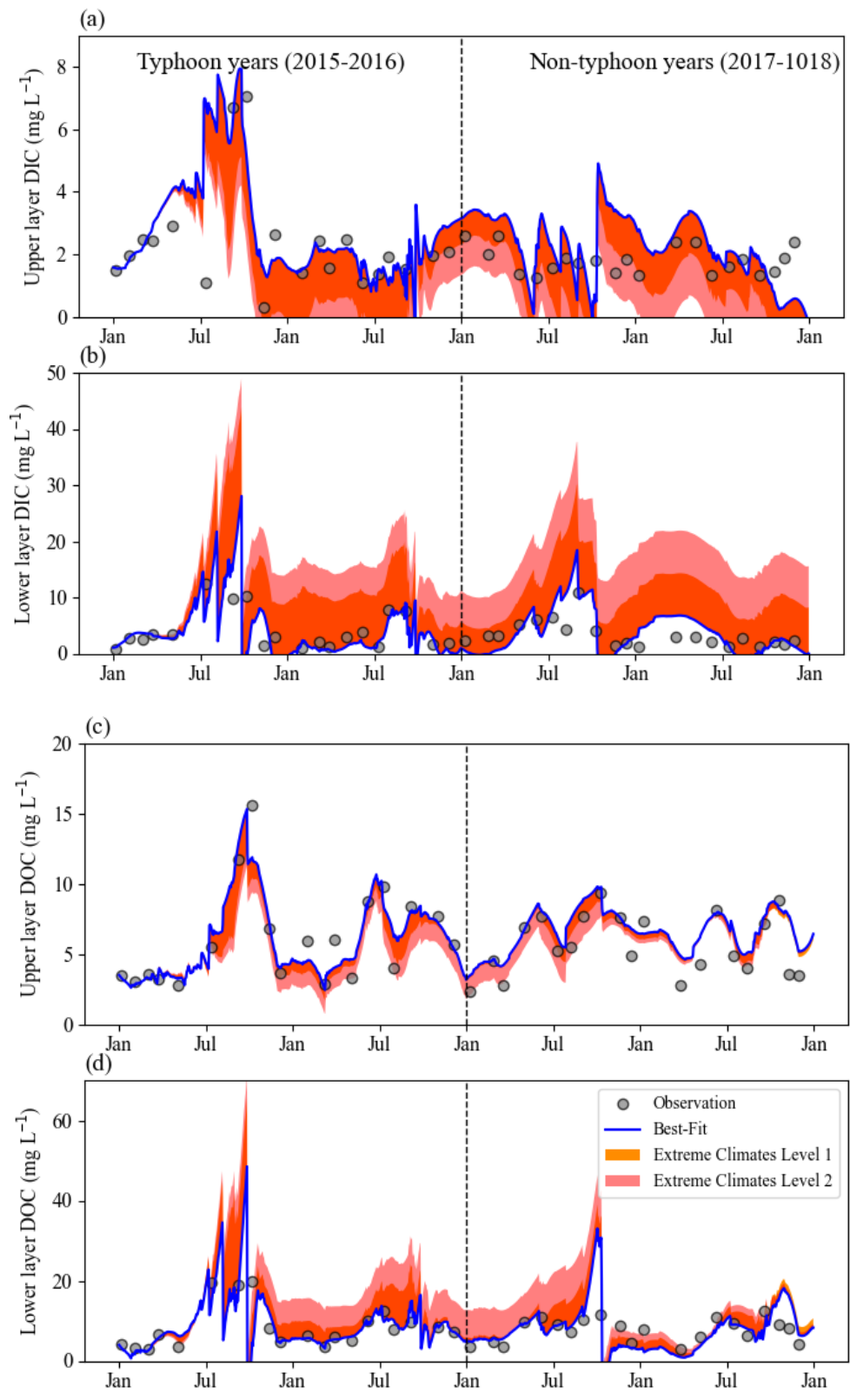
760
761 **Fig. 3.** Seasonal variations of (a) upper layer DIC (DIC_U), (b) lower layer DIC (DIC_L),
762 (c) upper layer DOC (DOC_U), (d) lower layer DOC (DOC_L), (e) upper layer Chl. a
763 (Chl_U), (f) lower layer Chl. a (Chl_L) grouped by typhoon and non-typhoon years. The
764 bullet points show the water sampling data. To determine seasonality, we used one-way
765 ANOVA to obtain the p -values. “ns”: p -values ≥ 0.05 ; * show p -values from 0.05 to
766 0.01; **: p -values from 0.01 to 0.001.
767



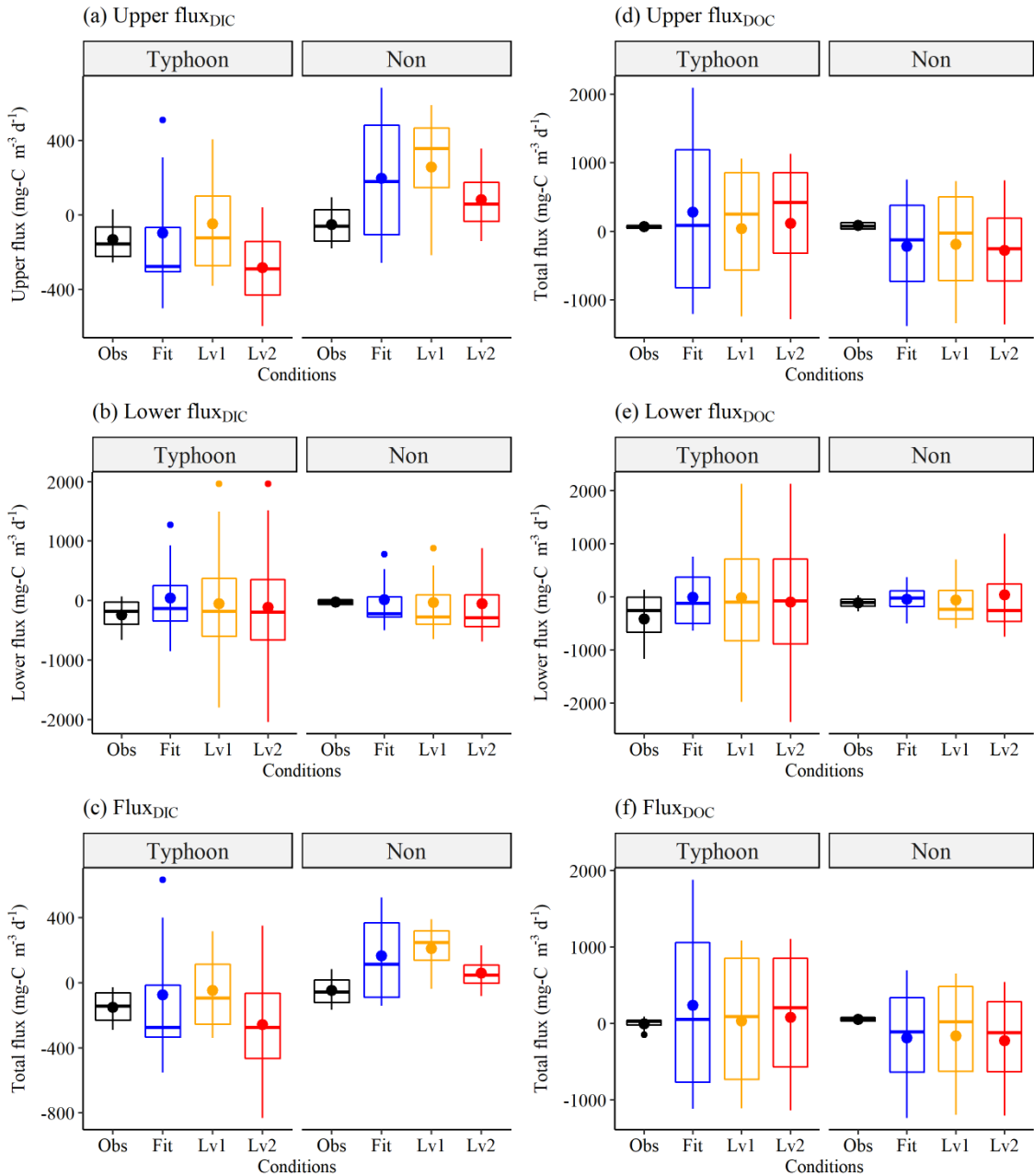
768

769 **Fig. 4.** Pearson correlation coefficients of DIC, DOC, and Chl. a concentration at upper
770 layer and lower layer DIC (DIC_U , DIC_L), DOC (DOC_U , DOC_L), Chl. a (Chl_U , Chl_L)
771 during (a) typhoon years and (b) non-typhoon years. Black-crosses show insignificant
772 values (p -values are > 0.05).

773

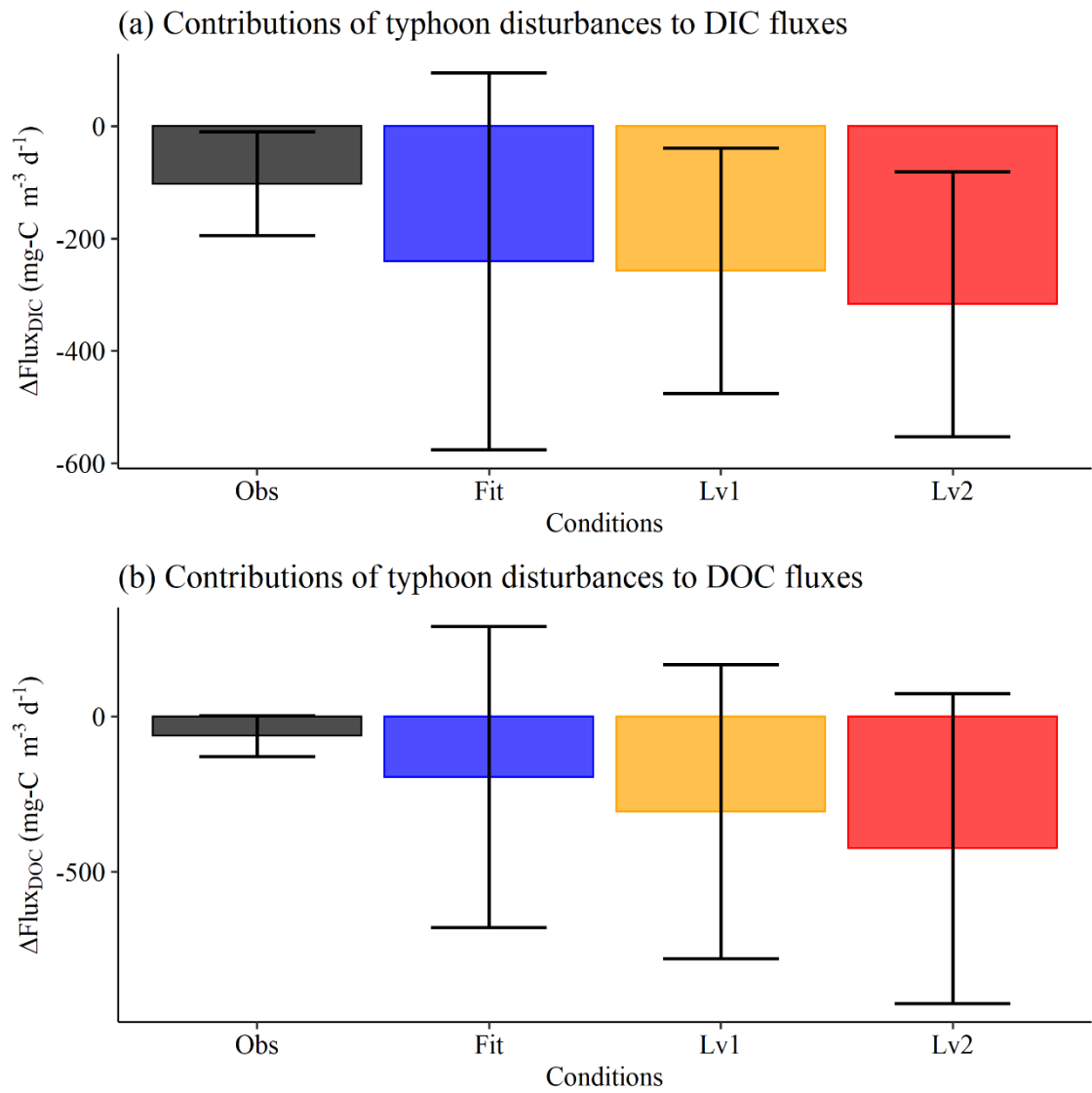


778 **Fig. 5.** Continuous daily DIC and DOC data at **(a, c)** upper layer (DIC_U , DOC_U) and **(b,**
779 **d)** lower layer (DIC_L , DOC_L) by using the conceptual equation model under extreme
780 climates from 2015 to 2018. *Blue lines* are original best-fit data, in which the
781 parameters of the DIC model in non-typhoon years are as shown in Table 3, and *gray*
782 *dots* show water sampling (observation) data for each month ($n = 41$) from January
783 2015 to December 2018. *Orange regions* show *Level 1*; *pink regions* show *Level 2*.



784
785 **Fig. 6.** Interannual (a) Upper flux_{DIC}, (b) Lower flux_{DIC}, (c) Flux_{DIC}, (d) Upper flux_{DOC},
786 (e) Lower flux_{DOC}, and (f) Flux_{DOC} ($\text{mg C m}^{-3} \text{d}^{-1}$) grouped by typhoon and non-typhoon
787 years. The *Obs* condition (*black boxes*) show the observation data as in Fig. 5. The *Fit*
788 condition (*blue- boxes*) shows the best-fit data by using the conceptual two-layer carbon
789 model as in Fig.5. *Level 1* (*yellow boxes*) and *Level 2* (*red boxes*) show the extreme
790 scenarios as in Fig. 6. For the definitions of fluxes please see Sect. 2.3.3. Positive values
791 are shown in the carbon sink, and negative ones show the values after carbon was released
792 within YYL.

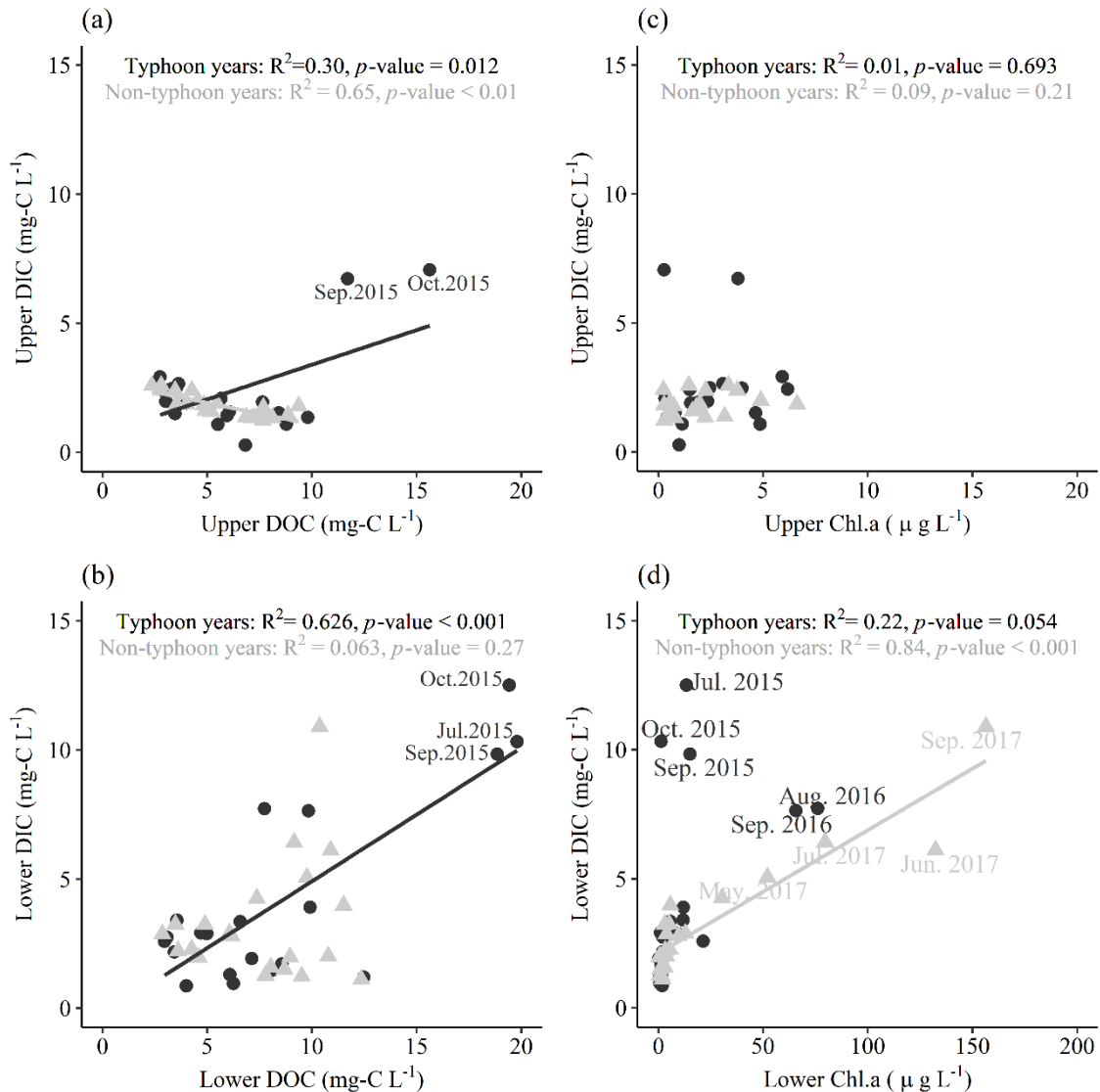
793



794

795 Fig. 7. Contributions of typhoon disturbances to (a) DIC and (b) DOC fluxes ($\text{mg-C m}^{-3} \text{ d}^{-1}$).
 796 Contributions of typhoons to C fluxes ($\Delta\text{Flux}_{\text{DIC}}$, $\Delta\text{Flux}_{\text{DOC}}$) represented the intervals of
 797 Flux_{DIC} (or Flux_{DOC}) in typhoon years and non-typhoon years (e.g., $\Delta\text{Flux}_{\text{DIC}} = \text{Flux}_{\text{DIC}}$ in
 798 typhoon years – Flux_{DIC} in non-typhoon years).

799



800
801 Fig. 8. Interactions of measurements data in typhoon years and non-typhoon years. The *black*
802 *circles*: typhoon years, *gray triangles*: non-typhoon years. The solid lines represent the linear
803 regression line in typhoon years (*black lines*) and non-typhoon years (*gray lines*).
804